ECLÉTICA QUÍMICA

Eclet. Quim. 50 | e-1600, 2025

Original Article

https://doi.org/10.26850/1678-4618.eq.v50.2025.e1600

Phytochemical, antioxidant, and enzyme inhibition potential exploration of *Nyctanthes arbor-tristis via in vitro* and *in silico* methods

Nirmal **Parajuli**[1], Prabhat **Neupane**[1], Sujan **Dhital**[1], Samjhana **Bharati**[1], Timila **Shrestha**[1], Binita **Maharjan**[1], Bishnu Prasad **Marasini**[2], Jhashanath Adhikari **Subin**[3], Ram Lal Swagat **Shrestha**[1,4+]

Abstract

Secondary metabolites in medicinal plants have been found to possess a broad spectrum of therapeutic properties. This study investigates the sequential extraction, quantitative phytochemicals, and bioactivity evaluations of Nyctanthes arbor-tristis leaf growing in Nepal. Methanolic extract contains the highest phenolics and resulted in the lowest IC50 values of 56±3 µg/mL and 157±3 µg/mL, in antioxidant and α-amylase inhibition assays, respectively. Hexane extract was found to contain abundant flavonoids and to be the most lethal to brine shrimp napuili with LC50 of 87±5 µg/mL. Phytochemicals arborside-C (ASC) and arborside-D (ASD) were found to be the most potent ligands to bind with α-amylase (PDB ID: 4GQR), resulting from docking and molecular dynamics simulation outcomes. The free energy changes calculated by the MMPBSA method and ADMET profiling of hit candidates supported by the spontaneity of complex formation reactions and their pharmacokinetic efficacy, respectively. This study proposes two compounds as hit candidates for the α-amylase target. Biological characterization using an in vivo approach is further recommended to assess their precise pharmacological validation.

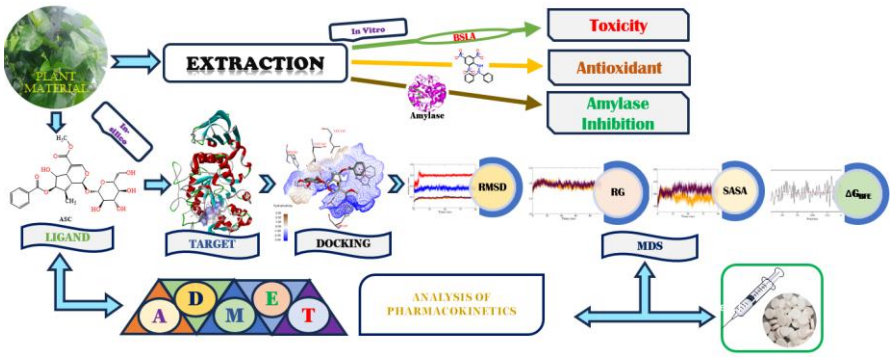

Article History

Received	September 19, 2024
Accepted	January 15, 2025
Published	September 22, 2025

Keywords

1. *Nyctanthes arbor-tristis;*
2. antioxidant;
3. α-amylase inhibition;
4. arborside-C;
5. arborside-D.

Section Editors

Assis Vicente **Benedetti**

Rogéria Rocha **Gonçalves**

Highlights

- Ultrasonic sequential extraction of phytochemicals from *N. arbor-tristis* leaf.
- Quantitative phytochemical study (TPC and TFC).
- Assessment of in vitro antioxidant, toxicity, and α-amylase inhibition bioactivities.
- Molecular docking and molecular dynamics simulations (MDS) of phytocompounds.
- Identification of hit compounds against pancreatic amylase through in silico methods.

[1]Tribhuvan University, Department of Chemistry, Kathmandu, Nepal. [2]Ministry of Health and Population, Nepal Health Research Council, Kathmandu, Nepal. [3]Bioinformatics and Cheminformatics Division, Scientific Research and Training Nepal P. Ltd., Bhaktapur, Nepal. [4]Institute of Natural Resources Innovation, Kathmandu, Nepal.
+Corresponding author: Ram Lal Swagat Shrestha, **Phone:** +9851038789, **Email address:** swagatstha@gmail.com

1. Introduction

Nepal is home to a wide array of plants, with an estimated 9,000 different species of flowering plants (Khakurel *et al.*, 2022; Kunwar *et al.*, 2016). Plants have medicinal values due to secondary metabolites and are a good source of therapeutics (Kumar *et al.*, 2022). Biosynthesis, extraction, identification, structural elucidation, quantification, and physical and chemical properties of phytochemicals are the key to the drug discovery process (Butler, 2004; Choo and Chai, 2023).

Nyctanthes arbor-tristis L., a plant of the Oleaceae family, commonly called Night jasmine, is a typical shrub with bright, highly scented blooms that bloom at night and fall off before daybreak (Dewi *et al.*, 2022). The plant is 10 to 30 m in height, and its leaves are 2–6 cm broad, 6–12 cm long, simple, petiolate, exstipulate, and reticulate venation (Solanki *et al.*, 2021). *N. arbor-tristis* is distributed worldwide and found in tropical and subtropical regions, ranging in height up to 1500 m geographically in the Himalayan region of India, Nepal, and Pakistan (Jain and Pandey, 2016).

N. arbor-tristis leaves have a variety of chemical components, including alkaloids, glycosides, flavonoids, terpenoids, and tannins (Bb *et al.*, 2015; Meshram *et al.*, 2012). The therapeutic benefit is related to the presence of possible phytochemicals such as nyctantic acid, β-sitosterol, oleanolic acid, friedelin, arborside-A, arborside-B, arborside-C, arborside-D, arbortristoside-A, arbortristoside-C, benzoic esters of loganin, 6-β-hydroxyloganin, mannitol, astragalin, ascorbic acid, and methyl salicylate found in the leaves (Agrawal and Pal, 2013; Sah and Verma, 2012; Meshram *et al.*, 2012). The pharmacological studies showed their potential as antibacterial, anti-inflammatory, analgesic, antidiabetic, cough-suppressant, antioxidant, antimalarial, anti-arthritic, antispasmodic, antipyretic, immunostimulant, anthelminthic, antileishmanial, hepatoprotective, anti-allergic, antiviral, and CNS depressive (Sah and Verma, 2012; Laware and Shirole, 2023; Rawat *et al.*, 2021). Each component of this plant has been used to treat various ailments in Ayurveda, including arthritis, digestive issues, tonics, laxatives, diuretics, asthma, cough, discomfort, hemorrhoids, and irregular menstrual periods (Dewi *et al.*, 2022; Kushwah *et al.*, 2023).

Diabetes Mellitus (DM), type I and II are chronic hyperglycemia disorders. Type I diabetes is caused mainly by β-cell death of the pancreas that results in a reduction in insulin secretion, in contrast, type II diabetes (T2D) is characterized by insulin resistance in the cells (Mohamed *et al.*, 2023). The ingestion and absorption of dietary carbohydrates substantially increase postprandial blood glucose levels (Sugandh *et al.*, 2023). The enzyme α-amylase breaks down starch into glucose fragments by breaking down the glycosidic linkages (Proença *et al.*, 2019). Human pancreatic α-amylase enzyme (HPAE) inhibition is a conventional method utilized to treat T2D (Ogunyemi *et al.*, 2022). An *in silico* methodology has effectively decreased the expenditure associated with experimental procedures and the temporal requirements for determining complicated structures (Stănciuc *et al.*, 2020). It aims to ascertain the potential method of binding orientation, binding affinity, and stability of the molecules to enzymes (Vasanthkumar *et al.*, 2021). Molecular docking calculations and molecular dynamics simulations are used to test millions of possible binding orientations at receptor binding sites based on protein structures to propose the pharmacological significance of various chemicals in plant metabolites (Hollingsworth and Dror, 2018; Zhao *et al.*, 2021). The structure-based drug design (SBDD) utilizes docking and simulation programs for virtual estimation of drug-likeness, and further ADMET prediction anchors to drug-like molecules through its pharmacokinetic evaluation that binds with a particular receptor protein to manipulate its function (Lolok *et al.*, 2022).

In this study, an assessment of the *in vitro* antioxidant, α-amylase inhibition, brine shrimp lethality assay (BSLA), and estimation of TPC and TFC of the different extract fractions of *N. arbor-tristis* leaf were carried out. Molecular docking virtual screening, molecular dynamics simulations, and ADMET predictions of the compounds found in the plant leaf were further used to understand their mechanism and pharmaceutical aptitude towards HPAE. The result of this study can be used to justify and validate the potential of the *N. arbor-tristis* in antioxidation, cytotoxicity, and, importantly, α-amylase inhibition.

2. Experimental

2.1. Chemicals

Solvents hexane, chloroform, ethyl acetate, acetone, methanol (Qualigens Fine Chemicals), sulfuric acid, hydrochloric acid, aluminum chloride, sodium carbonate, dimethyl sulphoxide (DMSO), and sodium dihydrogen phosphate (Thermo-Fisher Scientific India) were used. Gallic acid (Hi-media Laboratories), 2,2-diphenyl-1-picrylhydrazyl (DPPH), quercetin (Wako Pure Chemicals, Osaka, Japan), Folin–Ciocalteu's phenol reagent (FCR), ascorbic acid, acarbose, and α-amylase (Hi-media Laboratories) were used, which were imported from India.

2.2. Plant collection and identification

The *N. arbor-tristis* leaves were collected in Sindhupalchok district, Nepal (altitude: 1350 m, latitude: 27°46'14" N, longitude: 85°48'59" E). The plant (voucher code 01KATH160201) was identified and verified at the National Herbarium & Plant Laboratories (KATH) in Lalitpur, Nepal.

2.3. Preparation of plant extracts

The collected and dried 1 kg leaves of *N. arbor-tristis* were powdered using an electric grinder. Through an ultrasonic extraction process, different leaf extracts, hexane extract (**HE**), chloroform extract (**CE**), ethyl acetate extract (**EAE**), acetone extract (**AE**), methanol extract (**ME**), and distilled water extract (**DWE**), were prepared in six different solvents, hexane, chloroform, ethyl acetate, acetone, methanol, and distilled water, respectively through a sequential extraction (solid-liquid fractionation) in increasing polarity order of the solvents.

2.4. Preliminary phytochemical profiling

A phytochemical study of *N. arbor-tristis* leaf was conducted to profile the various natural constituents in the extracts using a standard protocol (Banu and Cathrine, 2015).

2.5. Phenolic content (TPC) determination

Folin-Ciocalteu colorimetric analysis based on an oxidation-reduction reaction was used to TPC with minor modifications (Gautam *et al.*, 2022). From the serially diluted concentration of standard gallic acid stock (500 to 25 µg/mL), 20 µL of each was dispensed in a 96-well plate containing 100 µL of Folin-ciocalteu reagent and incubated for 5 min at room temperature in the dark. 80 µL of 7% Na_2CO_3 was added to the

reaction mixture and further incubated for another 2 h at 23 °C. The resulting blue-colored mixture was subjected to measuring absorbance using a spectrophotometer at 765 nm in triplicate, and a calibration curve was plotted. The exact process was repeated for all plant extract fractions, and the TPC of each extract was calculated as gallic acid equivalent per gram (GAE/g) using a calibration curve.

2.6. Flavonoid content (TFC) determination

The aluminum chloride colorimetric assay was used to measure the TFC of the extracts described in previous work (Chandra *et al.*, 2014). Briefly, the stock solution of standard quercetin in methanol was serially diluted (250 µg/mL to 25 µg/mL) and added to the microplate well. 2% aluminum chloride in methanol (100µL) was added to it and incubated for 10 min in the dark. The absorbance of the reaction mixture was measured at 425nm through a spectrophotometer. The calibration curve was plotted, the exact process was repeated for all plant extract fractions, and TFC was calculated as quercetin equivalent per gram (QE/g).

2.7. Antioxidant activity assay

Using 2,2-diphenyl-1-picrylhydrazyl-hydrate (DPPH) (Blois, 1958), an antioxidant activity assay was done on the protocol described in previous literature, with some modifications (Sabudak *et al.*, 2013). The stock solution of standard ascorbic acid was resolved into concentrations of 30 µg/mL to 2.5 µg/mL through serial dilution. 2 mL of each concentration of ascorbic acid was mixed with 2 mL 0.2 mmol/L DPPH solution in triplicate and kept in the dark for 30 min. The absorbance was measured at 517 nm against methanol and DPPH as a blank. The exact process was repeated for each extract fraction (triplicate) at different concentrations, and absorbance was measured. Using a graph plot between the percentage scavenging activity of extracts vs concentrations in GraphPad Prism, the half-maximum inhibitory concentration (IC_{50}) of each extract was calculated. **Equation 1** was applied to evaluate the %DPPH radical scavenging.

$$\% \text{ DPPH Scavenging} = \frac{(A_{blank} - A_{sample})}{(A_{blank})} \times 100\% \quad (1)$$

2.8. α-Amylase inhibition assay

The α-amylase inhibition activity was performed using the 3,5-dinitrosalicylic acid (DNSA) method, with some modifications (Mustafa *et al.*, 2021). 10% dimethyl sulfoxide (DMSO) was used to dilute the *N. arbor-tristis* leaf extracts and generate various concentrations. The diluted solutions in different test tubes were mixed with DMSO, buffer, and NaCl at a pH of 6.9. This mixture was added with α-amylase (1,4-α-D-glucano-glucanohydrolase) solution (200 µL) and incubated for 10 min at a temperature of 30 °C. The starch solution (0.1%) was added to each tube in a volume of 200 µL, and the tubes were incubated for 3 min. The process was stopped by adding DNSA reagent (200 µL) and warmed in a water bath for 10 min at 85-90 °C. After reaching room temperature, the reaction mixture was diluted by adding distilled water (5 mL), and the absorbance of the reaction mixture was measured at 540 nm. The blank with 100% enzyme activity was prepared by replacing the plant extract with 200 µL of buffer. The standard acarbose solution was taken as a positive control. The percentage of amylase inhibition was estimated using **Eq. 2**.

$$\% \text{ inhibition} = \frac{Abs.blank - Abs.\ sample}{Abs.blank} \times 100\% \quad (2)$$

By plotting the extract concentrations against the percentage of α-amylase inhibition in the dose-inhibition curve using GraphPad Prism, the IC_{50} value was estimated for each extract.

2.9. Brine shrimp toxicity assay

The brine shrimp toxicity assay is a valuable introductory screening tool to determine the potential toxicity of various compounds (Niksic *et al.*, 2021). It involves assessing their potential to induce mortality in laboratory-cultured brine shrimp (*Artemia salina*) nauplii, and the protocol is based on previous work (Majumder *et al.*, 2019). Artificial seawater was prepared, and brine shrimp eggs were hatched for 48 h. A stock solution of each extract was successfully diluted (1000 µg/mL to 62.5 µg/mL) using the serial dilution method. Varying amounts of plant extract were applied to ten nauplii and left for 24 h. DMSO was used as a blank, and potassium dichromate as a positive control. The mortality endpoint was observed for each extract fraction after application to the prepared solution in a triplicate format. The lethality percentage for each concentration was determined by counting the number of dead and live nauplii. **Equation 3** was used to calculate the percentage mortality of the nauplii.

$$\% \text{ Mortality} = \frac{\text{No. of dead shrimps}}{\text{Total No. of shrimps}} \times 100\% \quad (3)$$

The LC_{50} represents the concentration at which the tested extract kills 50% of the brine shrimp nauplii. It was calculated using GraphPad Prism.

2.10. Computational tools

2.10.1. Ligand selection

The previously isolated compounds (iridoids, flavonoids, and phenolic compounds) from different extracts of the leaves of *N. arbor-tristis* were taken as candidate ligands as HPAE inhibitors (**Table 1**). Molecular structures of some of the selected ligands are presented in **Fig. 1**. The **Supplementary Information** (**Table 1S** and **Fig. 1S**) lists other detailed information and structures of all selected ligands.

Table 1. Some of the top candidate ligands selected from *N. arbor-tristis* leaf.

Ligands	Ligand ID	Molecular weight (g/mol)	PubChem CID	Reference
Arborside-A	ASA	614.6	182902	Dewi *et al.* (2022)
Arborside-B	ASB	494.5	182903	Dewi *et al.* (2022)
Arborside-C	ASC	510.5	182904	Agrawal and Pal (2013)
Arborside-D	ASD	556.5	101685135	Agrawal and Pal (2013)
Arbortristoside-A	ATSA	566.5	6442162	Vishwakarma *et al.* (2022); Rathore *et al.* (1989)
Arbortristoside-C	ATSC	552.5	23955893	Dewi *et al.* (2022)
Astragalin	AG	448.4	5282102	Sah and Verma (2012)

Source: Elaborated by the authors.

https://doi.org/10.26850/1678-4618.eq.v50.2025.e1600

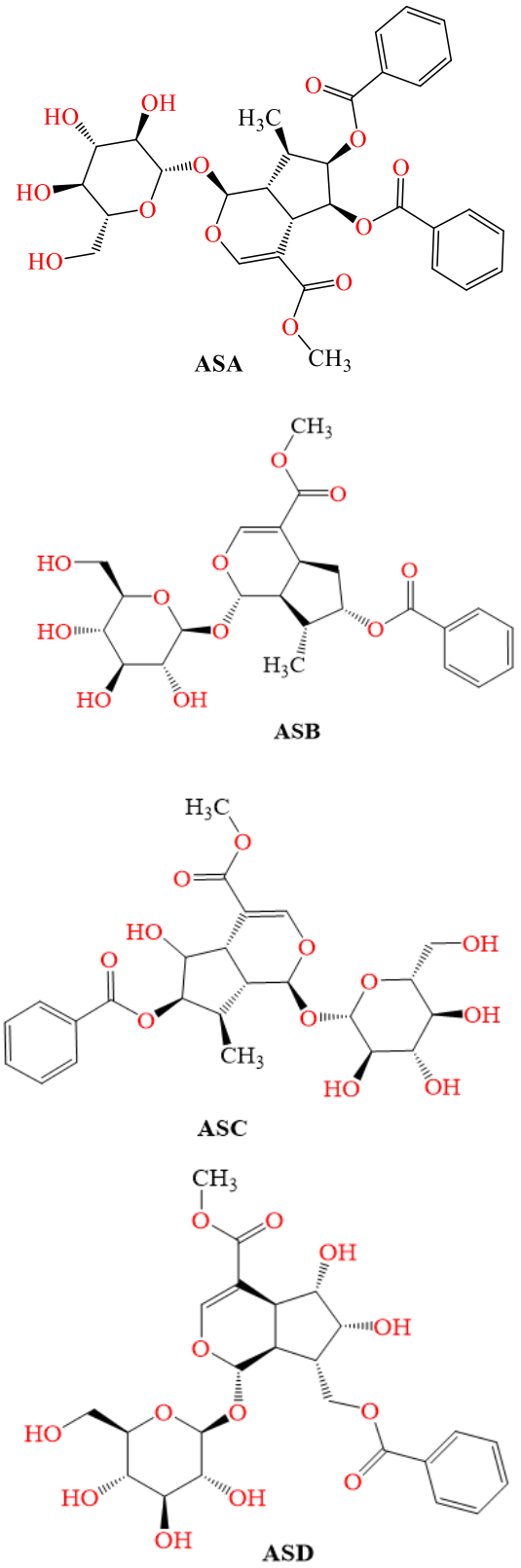

Figure 1. Molecular structures of some of the top selected ligands, **ASA** (Arborside-A), **ASB** (Arborside-B), **ASC** (Arborside-C), and **ASD** (Arborside-D).
Source: Elaborated by the authors.

2.10.2. Ligand preparation

The 3D structures and coordinates of ligands were retrieved from the PubChem database in sdf format with the respective PubChem CID mentioned in **Table 1**. The bond order and molecular formula of compounds were verified and converted into pdb format using the PyMOL software (version 2.5.5) (Yuan *et al.*, 2017). Using the conjugate gradient algorithm, the Universal Force Field (UFF) for 5000 cycles at 10^{-8} units of energy convergence was chosen after adding the hydrogen atoms in the Avogadro program (version 1.2.0) for molecular structure optimization (Hanwell *et al.*, 2012). AutoDock Tools converted pdb into pdbqt, which is required for molecular docking (Trott and Olson, 2009). Root mean square deviation (RMSD) between the docked ligand (myricetin) and native ligand (myricetin) in the crystal structure of the protein (PDB ID: 4GQR) was calculated to be less than 2 Å for docking protocol validation (Shrestha *et al.*, 2024) (presented in **Fig. 2S** in **Supplementary Information**).

2.10.3. Target selection and preparation

HPAE (PDB ID: 4GQR) with a resolution of 1.20 Å, with an X-ray crystallographic structure, was restored from the RCSB database (**https://www.rcsb.org/**) (Berman *et al.*, 2000). The protein structure visualization and processing were done using the PyMOL program. The active sites (catalytic triad, ASP197, GLU233, and ASP300) of the enzyme were determined using a co-crystallized receptor-ligand complex structure (Liu *et al.*, 2017a). The protein was cleaned in PyMOL software by removing water molecules, ions, and non-standard residues, and the apo structure was stored as a pdb file. The protein was processed by adding polar hydrogen atoms and Kollman charges in AutoDock Tools and converted into pdbqt format, which was required for molecular docking. The grid box was set to cover all the active site residues. The grid box center (16.731, 17.235, and 42.467) and the grid box size (x = 44, y = 46, z = 44 in Å with spacing of 0.375 Å) in the receptor protein were selected.

2.10.4. Molecular docking calculations

The binding mechanism (pose, orientation, and location) between the ligand and the receptor was investigated using molecular docking studies. The AutoDock Vina software (version 1.5.7) was used to conduct rigid molecular docking calculations (Trott and Olson, 2009). The chosen molecules were docked and examined based on the possible protein-ligand interactions and the lowest binding affinity (docking score). During molecular docking, the ligand remained flexible in the active site pocket of the protein despite the protein's rigidity. Control parameters such as the number of modes, energy range, and exhaustiveness were 20, 4, and 64, respectively, for all docking computations. The stable protein-ligand complex with the highest binding affinity was ultimately determined using a scoring function. Biovia Discovery Studio Visualizer (version 21.1.0.20298) was used for the visualization of protein-ligand interactions (Shaweta *et al.*, 2021). For the stability assessment in terms of geometrical and thermodynamic parameters, a molecular dynamics simulation of the complex with the pose with the best binding energies was selected.

2.10.5. Molecular dynamics simulation (MDS)

The MDS of the ligand-protein adducts were performed using the GROMACS software (version 2021.2) (Abraham *et al.*, 2015). The Charmm27 force field from the swissparam server (**https://www.swissparam.ch/**) (assessed on January 10, 2024) was used for both the ligand and the receptor (Zoete *et al.*, 2011). Utilizing the TIP3P water model, a triclinic box system was solvated. 12 Å spacing was chosen to minimize erroneous interactions between the periodic images. The system was

neutralized, and an isotonic solution of NaCl was employed. At a physiological temperature (310 K), the system was equilibrated in four stages, each lasting 200 ps. For NVT equilibrium, the initial two stages were completed, and for NPT equilibrium, the final two phases were chained. The final production run was conducted for 100 ns without any constraints, and several parameters, including RMSF, SASA, RMSD, and R_g, were retrieved from the MDS trajectory using the built-in modules of the GROMACS program.

2.10.6. Binding free energy changes (ΔGBFE) estimation

The MMPBSA method was used to calculate the change in the binding free energy (ΔG_{BFE}) of the adduct (Onufriev and Case, 2019). The viability and spontaneity of the forward reaction were evaluated based on the assessment of free energy changes. The binding free energies of the complex, protein, and ligand were determined using the gmx-MMPBSA module on an equilibrated trajectory segment of 200 frames for 20 ns. **Equations 4** and **5** were used to calculate the binding free energy change during complex formation (Wang *et al.*, 2019).

$$\Delta G_{BFE} = G_{complex} - G_{receptor} - G_{ligand} \quad (4)$$

$$\Delta G_{BFE} = \Delta H - T\Delta S = \Delta E_{MM} + \Delta G_{SOLV} - T\Delta S \quad (5)$$

where,
$\Delta E_{MM} = \Delta E_{IN} + \Delta E_{vdw} + \Delta E_{ELE}$
$\Delta G_{SOLV} = \Delta G_{PB} + \Delta G_{SA}$
ΔG_{BFE} = Binding Free Energy changes
ΔE_{MM} =Energy change in gas phase molecular mechanics
ΔE_{IN} = Internal energy of the system
ΔE_{vdw} = van der Waals energy
ΔG_{SOLV} = Electrostatic solvation energy
ΔG_{PB} = Polar contributions in solute-solvent system
ΔE_{ELE} = Electrostatic energy
ΔS = Entropy changes of the system
ΔG_{SA} = Nonpolar contributions in the system

The entropy term ($T\Delta S$) was not considered in the binding free energy calculation because of significant technical costs and errors raised during computational calculations (Wang *et al.*, 2019).

2.11. ADMET profiling

Swiss ADME (**http://www.swissadme.ch/**), ProTox-II (**https://tox-new.charite.de/protox_II/**), and pkCSM (**https://biosig.lab.uq.edu.au/pkcsm/**) servers (accessed on January 19, 2024) were used for calculating absorption, distribution, metabolism, excretion, and toxicity parameters of hit compounds and reference drugs (Acarbose and Miglitol) (Banerjee *et al.*, 2018; Pires *et al.*, 2015).

2.12. Statistical evaluation

All the *in vitro* experimental results were taken in triplicate (n = 3). TPC, TFC, and binding free energy results were presented as mean ± SD (standard deviation), and quantitative biological activity tests (DPPH assay, amylase inhibition, and BSLA) were calculated in terms of mean ± SEM (standard error of mean) for a more reliable IC_{50} calculation. GraphPad Prism (version 9.4.1) was used to calculate IC_{50} values of bioactivities. TPC and TFC were calculated using Microsoft Excel 2021.

2.13. Computational resources

Molecular docking calculations, data interpretation, and visualization were done using Windows 11 (8 GB RAM, 8-core CPU processor). Molecular dynamics simulation and binding free energy calculations were performed in Ubuntu 20.04.06, an LTS operating system, a 24-core processor machine with a 24 GB GPU accelerator.

3. Results and discussion

3.1. Qualitative estimation of phytochemicals

Qualitative analysis of the phytochemicals gives a preliminary idea of constituents present in the extracts and helps to quantify and further characterize (Olayinka *et al.*, 2010). The FT-IR analysis of the extract is presented in the **Supplementary Information** in **Fig. 3S**. Different extracts showed distinct results in screening following polarity and phytoconstituents present in the leaf of *N. arbor-tristis*. Alkaloids, flavonoids, terpenoids, glycosides, phenolic compounds, steroids, carbohydrates, and quinones were identified (**Table 2**) as the primary ingredients.

Table 2. Phytochemical screening of the various extracts.

Class of phytochemicals	HE	CE	EAE	AE	ME	DWE
Alkaloids	–	+	+	+	+	+
Phenolic Compounds	–	+	+	+	+	+
Flavonoids	–	+	+	+	+	+
Terpenoids	+	+	+	+	+	–
Cardiac Glycosides	–	–	+	+	+	+
Carbohydrates	–	+	+	+	+	+
Proteins	–	–	+	+	+	+
Triterpenoids	+	+	+	+	–	–
Tannins	–	+	+	+	+	+
Resins	–	–	–	+	+	+
Steroids	–	+	+	+	+	–
Quinones	+	+	+	+	+	–
Saponins	–	–	–	–	–	–

Note: + refers presence; – refers absence. **HE** (Hexane extract); **CE** (Chloroform extract); **EAE** (Ethyl acetate extract); **AE** (Acetone extract); **ME** (Methanol extract); **DWE** (Distilled water extract).
Source: Elaborated by the authors.

3.2. Quantitative estimation of phytochemicals

The yield percentage was found to be the highest for the extract **CE** (7.3%) among all extract fractions. Phenolic compounds and flavonoids are natural products that have the potential for pharmacological activity, like antioxidant, antidiabetic, anti-inflammatory, and Anticarcinogen (Zain and Omar, 2018). TPC of different fractions was determined using Folin-Ciocalteu reagent with slight modification with the help of a standard gallic acid calibration curve (Y = 0.0039X + 0.0568, and R^2 = 0.9957), likewise, TFC was calculated through spectrophotometry of the colored solution of aluminum chloride reagent with extract with the help of a standard quercetin calibration curve (Y = 0.0068X + 0.00704, and R^2 = 0.9997). The standard calibration curves are included in the **Supplementary Information** (**Fig. 4S**). The % yield, TPC, and TFC of all fractions are listed in **Table 3**. Extracts of **AE** and **ME** fractions of *N. arbor-tristis* were found to have a high content of the phenolic compound of 137±4 mg GAE/g and 139±4 mg GAE/g, respectively. TFC was found high in extract **CE** (369 ± 4 mg GAE/g) and **HE** (286 ± 10 mg GAE/g) fractions.

Table 3. The yield, TPC, and TFC of different extract fractions.

Extracts	Chemical contents		
	Yield%	TPC (mg GAE/g)	TFC (mg QE/g)
HE	0.45	18 ± 4	286 ± 10
CE	7.3	46 ± 4	369 ± 4
EAE	1.55	78 ± 5	92 ± 4
AE	2.3	137 ± 4	62 ± 3
ME	3.15	139 ± 4	68 ± 4
DWE	2.97	56 ± 4	17 ± 2

Note: TPC and TFC = triplicate average ± SD. **HE** (Hexane extract); **CE** (Chloroform extract); **EAE** (Ethyl acetate extract); **AE** (Acetone extract); **ME** (Methanol extract); **DWE** (Distilled water extract).
Source: Elaborated by the authors.

3.3. DPPH scavenging assay

The DPPH radical scavenging assay gives the *in vitro* quantitative figure of the antioxidant potential of metabolites found in phytochemicals (Sethi *et al.*, 2020). *N. arbor-tristis* extract fractions displayed active antioxidant potentials towards DPPH free radicals. Extracts **ME** and **AE** were found to be the most potent antioxidants with IC_{50} values of 56 ± 3 g/mL and 79 ± 3 µg/mL, respectively, which were found to be marginally higher IC_{50} values than standard ascorbic acid (**Table 4**). Other extracts (IC_{50} > 100 µg/mL) showed mild antioxidizing phenomena. The order of the DPPH scavenging capacity of the extracts can be illustrated as **ME>AE>DWE>EAE>HE>CE**.

Table 4. Comparative antioxidant, amylase inhibition, and toxicity results containing values of various extracts with respective positive control.

Extracts and positive controls	Evaluated bioactivity		
	DPPH scavenging (IC_{50} in µg/mL)	α-Amylase inhibition (IC_{50} in µg/mL)	Brine shrimp lethality assay (LC_{50} in µg/mL)
HE	120 ± 5	547 ± 9	97 ± 2
CE	410 ± 6	386 ± 15	295 ± 7
EAE	126 ± 2	1656 ± 8	161 ± 5
AE	79 ± 3	919 ± 9	240 ± 5
ME	56 ± 3	157 ± 3	175 ± 3
DWE	104 ± 6	1799 ± 7	998 ± 10
***Ascorbic acid**	17 ± 3	–	–
***Acarbose**	–	52 ± 1	–
***$K_2Cr_2O_7$**	–	–	152 ± 2

Source: Elaborated by the authors.

3.4. Alpha-amylase inhibition assay

The α-amylase inhibition activity of different extracts is listed in **Table 4**. Among the fractions, **ME** of IC_{50} 157 ± 3 **µg/mL** was found to be a significant α-amylase inhibitor compared to other fractions. Extracts **HE** and **CE** exhibited moderate inhibition, whereas **EAE**, **AE**, and **DWE** showed weak inhibitory activity to the amylase enzyme. The extract **ME** showed a good amylase inhibition activity compared with standard acarbose (52 ± 1 µg/mL), signifying the antidiabetic potential of *N. arbor-tristis*. The amylase enzyme inhibition potential of the extracts was found to be in the following order: **ME > CE > HE > AE > EAE > DWE**.

3.5. Brine shrimp toxicity evaluation

Brine shrimp cytotoxicity assay portrayed a moderate toxicity in all extracts. LC_{50} of **HE** (97 ± 2 µg/mL) was found to be the least toxic to brine shrimp larvae. LC_{50} values of extracts **CE**, **EAE**, **AE**, and **ME** were found to be moderate, and comparable to each other and the positive control potassium dichromate (LC_{50} < 300 µg/mL). The comparative illustration of all the extracts with lethal concentration is mentioned in **Table 4**.

The trending fitting curve of the observed data of different bioactivity is presented in **Figures 5S**, **6S**, and **7S** in **Supplementary Information**.

3.6. Computational virtual screening

3.6.1. Binding affinities from molecular docking calculation

The most conventional method to inhibit HPAE is to bind it with a suitable ligand/drug at its orthosteric site (Cele *et al.*, 2022). Molecular docking is an easy, preliminary, virtual, and rapid computational method to compute and analyze the compatibility of any molecule (guest) and its possible therapeutic activity with the active macromolecular protein (host) through Host-Guest interaction (Das *et al.*, 2024). Further viability and stability of the docked complex were assessed using MDS. The compounds found in the leaves of *N. arbor-tristis* were examined to determine their HPAE binding capacity through computation. Most of the candidate ligands scored better in molecular docking than the native ligand myricetin (–33.1 kJ/mol) with the amylase receptor (PDB ID: 4GQR) (Bitew *et al.*, 2021), and the calculations are shown in **Table 5**. Conventional hydrogen bonds, Pi-alkyl, Pi-Pi stacked, other hydrophobic interactions, and van der Waals interactions were the noticeable non-covalent interactions in the protein-ligand complexes. Among all ligands, **ASC** and **ASD** scored the same affinity of –33.5 kJ/mol, and it was found that these ligands exhibited a stable trajectory in MDS, which might be a consequence of the strong interactions in the adduct with a larger hydrogen bond count and proper orientation of the ligand with the receptor. By conventional hydrogen bond, ligand ASC interacted with amino acid residues, HIS305, GLU233, ASP197, and ASP300 (<3 Å). On the other hand, ligand **ASD** interacted with TRP59, TYR151, THR163, and HIS 201 through hydrogen bonding (<2.6 **Å**) along with other possible interactions. Such strong interactions (between ligands and active site triad) might provide stability to the complexes, which were further supported by the MDS results of both ligands, which are discussed later. Although **ASB** showed the highest docking score (–34.7 kJ/mol), it was found to be unstable in the amylase binding pocket (in MDS). The docking score and its validity through MDS signified the stability of the adduct at physiological temperature, which could result in the inhibition of the target enzyme (Omar *et al.*, 2022). Most of the ligands were found to interact with the catalytic triad of amylase (**APS197**, **GLU233**, and **ASP300**), along with ASP356, HIS305, ILE235, HIS201, TRP59, ALA106, and ALA198 (Chothani *et al.*, 2024; Renganathan *et al.*, 2021; Zahra *et al.*, 2024).

Table 5. Interactions between the compounds (top ligands, drug, native ligand) and the amino acid residues in ligand-protein complexes from molecular docking calculations.

Candidate Ligands	Docking Score (kJ/mol)	Interactions	Active site residues (Distance Å)
ASB	**–34.7**	Conventional Hydrogen Bond	GLU233 (2.47, 2.66), ASP300 (2.12)
		Pi-Alkyl	TRP59 (4.38, 5.10), HIS305 (4.60)
		Carbon Hydrogen bond	HIS305 (3.77)
		Alkyl	LEU165 (4.74)
		van der Waals	TRP58, ASP197, TYR62, HIS201, GLN63, VAL107, LEU162, THR163, ARG195, ILE235,
ASC	**–33.5**	Conventional Hydrogen Bond	ASP197 (2.45), GLU233 (2.07), HIS305 (2.79), ASP300 (2.73)
		Alkyl	LEU162 (3.90), LEU165 (4.94)
		Pi-Alkyl	TRP59 (4.20), HIS305 (2.79)
		Pi-Pi Stacked	TRP59 (4.06)
		van der Waals	TRY62, TYR151, THR163, ARG195, GLN63, ALA198, TRP58, LYS200, ILE235
ASD	**–33.5**	Conventional Hydrogen Bond	TRP59 (2.14), TYR151 (2.57), THR163 (2.21), HIS201 (2.13, 2.58)
		Pi-Alkyl	HIS299 (4.38)
		Carbon Hydrogen bond	GLU233 (3.34), ASP300 (3.38)
		Pi-Pi Stacked	TYR151(3.93)
		van der Waals	TRP58, GLN63, LEU162, ARG195, ASP197, ALA198, GLU60, LYS200, TYR62, ILE235
ASTA	**–33.5**	Conventional Hydrogen Bond	GLU233 (1.84), ASP300 (2.23)
		Pi-Alkyl	HIS201 (5.16)
		Carbon Hydrogen bond	TRP59 (3.80), HIS299 (3.60)
		Pi-Pi Stacked	TRP59 (4.98)
		Pi-sigma	TRP59 (3.86)
		Alkyl	LEU162 (5.44), LEU165 (4.42), GLU233 (5.80)
		van der Waals	TRP58, TYR62, GLN63, TYR151, THR163, ARG195, ASP197, ALA198, HIS305, GLY306
AG	**–33.1**	Conventional H-Bond	GLN63 (2.82), ASP197 (4.43)
		Pi-Pi Stacked	TYR62 (5.08), TRP59 (4.03, 4.66)
		van der Waals	TRP58, GLN63, HIS101, LEU162, LEU165, ALA198, GLU233, ILE235, GLY306
		Pi-Alkyl	ALA307 (5.05)
		Carbon Hydrogen bond	TRP59 (3.24)
		Pi-Pi Stacked	TRP59 (5.16)
		Pi-sigma	ILE235 (3.93)
		Pi-Donor Hydrogen bond	HIS299 (3.28)
		van der Waals	TRP58, TYR62, GLN63, TYR151, LEU162, ARG195, ASP197, ALA198, LYS200, HIS305, GLY306, GLY308
#Myricetin	**–33.1**	Conventional H-bond	GLN63 (2.13), ARG195 (2.33), GLU233 (2.31)
		Pi-Pi staked	TRP59 (4.36, 5.39), TYR62 (4.83)
		Van der Waals	HIS101, LEU162, LEU162, ASP197, ALA198, HIS299, ASP300
***Acarbose Yi *et al.* (2022)**	**–32.2**	Conventional H-bond	GLN63 (2.33, 2.36, 2.62), ARG195 (3.04), GLU233 (1.98, 2.33), ASP300 (2.35)
		Pi-donor hydrogen bond	TRP59 (3.78, 3.88)
		van der Waals	VAL49, ILE51, TRP58, TYR62, LEU162, THR163, ASP197, ALA198, HIS299, PHE256, GLY306, GLY306, ARG303, HIS305, TRP357

Note: #Native ligand; *Antidiabetic reference drug. **ASB** (Arborside-B); **ASC** (Arborside-C); **ASD** (Arborside-D); **ATSA** (Arbortristoside-A); **ATSC** (Arbortristoside-C); **Bold residues** (catalytic triad residues in the orthosteric side of Human pancreatic *α*-amylase).
Source: Elaborated by the authors.

The observations indicated that the conventional hydrogen bond between electronegative acceptor and hydrogen, Pi-Pi stacked link between two aromatic rings, Pi-alkyl interaction between the alkyl group and aromatic ring or unsaturation, van der Waals' interaction, and other noncovalent interactions were found to be present between ligand and protein complexes. Ligand **ASC** formed H-bonds with active site residues GLU233 (H-acceptor), ASP197 (H-acceptor), and ASP300 (H-acceptor) by accepting the hydrogen from the H-donor (–OH) site of the ligand, and residues HIS201 (H-donor) and HIS305 (H-donor) donated the hydrogen to the acceptor oxygen site of the ligand. LEU162, LEU165, TYR59, and HIS305 interacted with ASC to bind by hydrophobic interactions containing Pi-Pi stacking, Pi-alkyl, and alkyl-alkyl interactions. Similarly, in ligand ASD, residues TRP59 and THR163 acted as hydrogen acceptors. HIS201 and TYR153 played a role as hydrogen donors in forming hydrogen bonds, and residues HIS299 and TYR153 showed hydrophobic interaction with the ligand. Docking scores and interactions of the ligands displayed the potential binding capability of the ligands towards HPAE, which could eventually be the subsequent inhibitory action of compounds in physiological reactions. The comparison (docking score and interactions) of selected compounds with native ligand (myricetin) and the drug acarbose (–32.2 kJ/mol) further supported the effective interactions and stability of the complexes formed with amylase enzyme. Figurative (3D interaction with the hydrophobicity of protein and solvent accessibility surface (SAS) in 2D) illustrations of molecular docking calculations of major active compounds are presented in **Fig. 2**. Other calculated data and figures are included in the supplementary information (**Tables 1S**, **2S**, and **Fig. 8S**).

https://doi.org/10.26850/1678-4618.eq.v50.2025.e1600

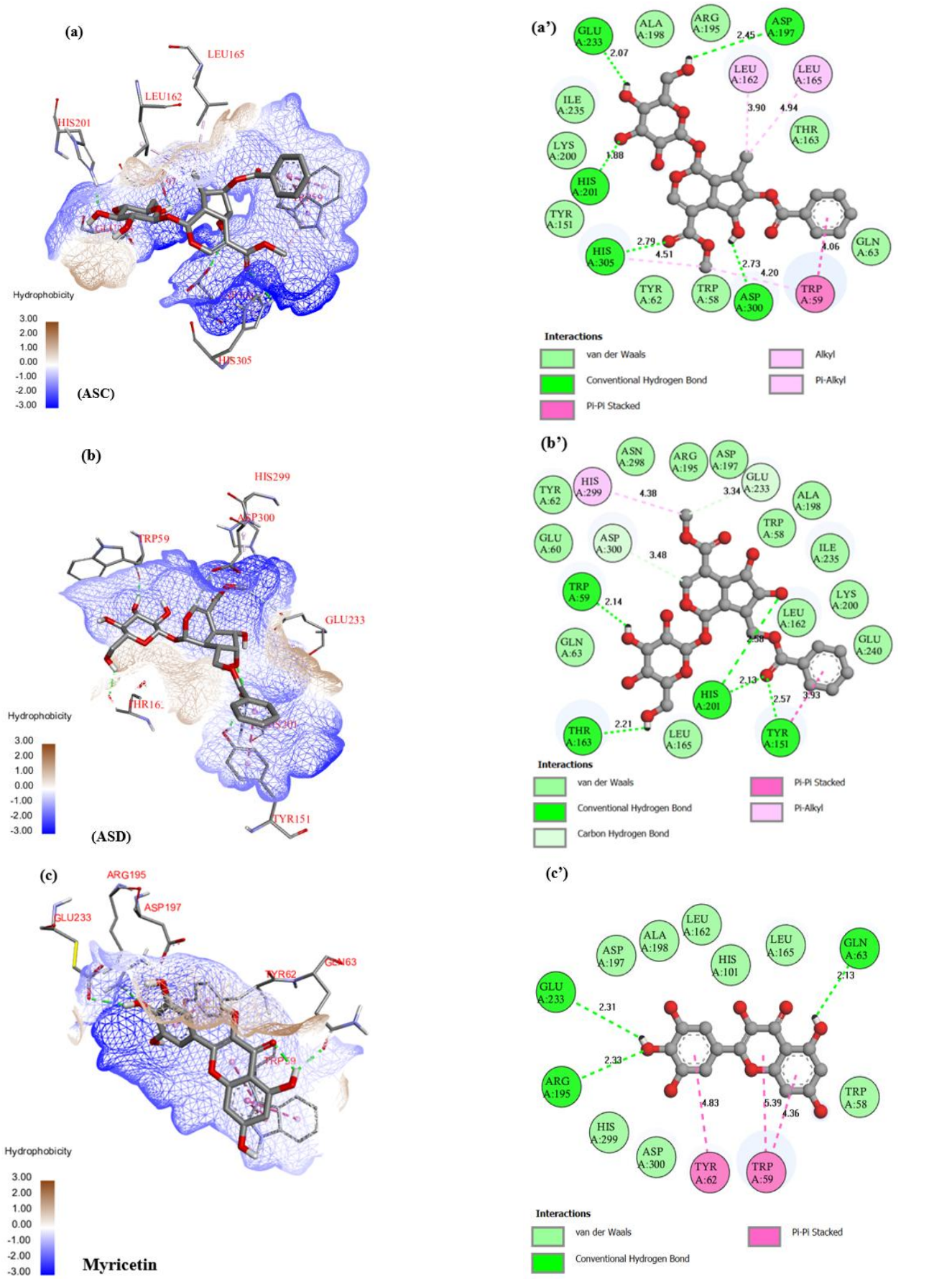

Figure 2. Interactive presentations of the protein-ligand complex of {(ASC **(a, a')**, ASD **(b, b')** and Myricetin **(c, c')**} 3D with the hydrophobicity of protein and 2D with solvent accessibility surface from molecular docking including bond length **(Å)**, the color of atoms in the ligand 2D structure, red, black, and grey are for **O**, **H**, and **C** atoms, respectively.
Source: Elaborated by the authors.

https://doi.org/10.26850/1678-4618.eq.v50.2025.e1600

3.6.2. Molecular dynamics simulations (MDS)

3.6.2.1. Root mean square deviation (RMSD)

MDS trajectory was used to extract the RMSD of ligand and protein for a duration of 100 ns, and it was considered to compute the dynamics and stability of the simulated complex (Adcock and McCammon, 2006). The stability of the simulated complex is assessed by the ligand and protein backbone RMSD and the smoothness of curves (Aier *et al.*, 2016). Among the selected compounds, **ASC** and **ASD** displayed better simulation results as they showed a stable trajectory (**Fig. 3a**) with a value below 6 Å. The protein backbone curves were lower than those of the ligand, indicating that the receptor's geometry remained stable throughout the MDS. The ligand binding to the receptor did not change the 3D structure of the adduct throughout 100 ns of the simulation time. The compound **ASC** depicted a smooth trajectory with an RMSD lower than 6 Å, but the RMSD for **ASD** was stable below 4 Å. The stability of the trajectory of the protein backbone in complexes (RMSD 1.8 nm) and apo structure (RMSD 1.5 nm) was found to support posture conservation, and the stability of the ligands during simulation at the binding site of the protein suggests their good inhibition potential towards the HPAE. A comparative and figurative presentation of the RMSD of ligand and protein backbone relative to the protein backbone in the protein-ligand complexes is given in **Fig. 3**.

3.6.2.2. Root mean square fluctuation (RMSF)

RMSF measures the fluctuation of alpha carbon atoms and conformational changes of the protein backbone during the MDS (Martínez, 2015). **Fig. 3c** presents the RMSF of alpha carbon atoms of the protein backbone in the **ASC** and **ASD** complexes. A larger RMSF may account for the RMS deviation (Martínez, 2015). Small RMSF peaks and fluctuations (helix and sheet structure of protein) on most of the catalytic sites and binding catalytic triad (ASP197, GLU233, and ASP300) signified the binding of the ligands **ASC** and **ASD** to the protein, which indicated the effective interaction of ligands at the active site and provided rigidity to the fluctuation of the protein backbone. The unusual rise of the curve at residue numbers up to 0.6 nm around 56, 310, 350, and 460 might be caused due to the presence of fluctuating loops at a larger distance.

3.6.2.3. Radius of gyration (Rg)

The radius of gyration (R_g) focuses on the conformational change in the simulated protein-ligand complex from MD simulation, as shown in **Fig. 3d**. R_g provides the average separation between all dispersed elements from the molecule's central axis (Liu *et al.*, 2017b). The correlation between RMSD, RMSF, and R_g provides insight into the relationship between complex compressibility, delocalization of the ligand, and residual fluctuations. Low RMSD, the rigidity of protein residues at binding sites, and the unchanging R_g support the stability of the complex formed. The R_g was nearly constant at about 2.34 nm for both complexes and the apo structure (**Fig. 9S**), roughly equal to the Rg before complexes formed (2.35 nm). The minimal variation in R_g suggested no appreciable deformation of the receptor's geometry and compactness upon the binding of ligands (Ahmed *et al.*, 2022). Therefore, the adducts of **ASC** and **ASD** with HPAE remained stable in terms of compactness during the MDS.

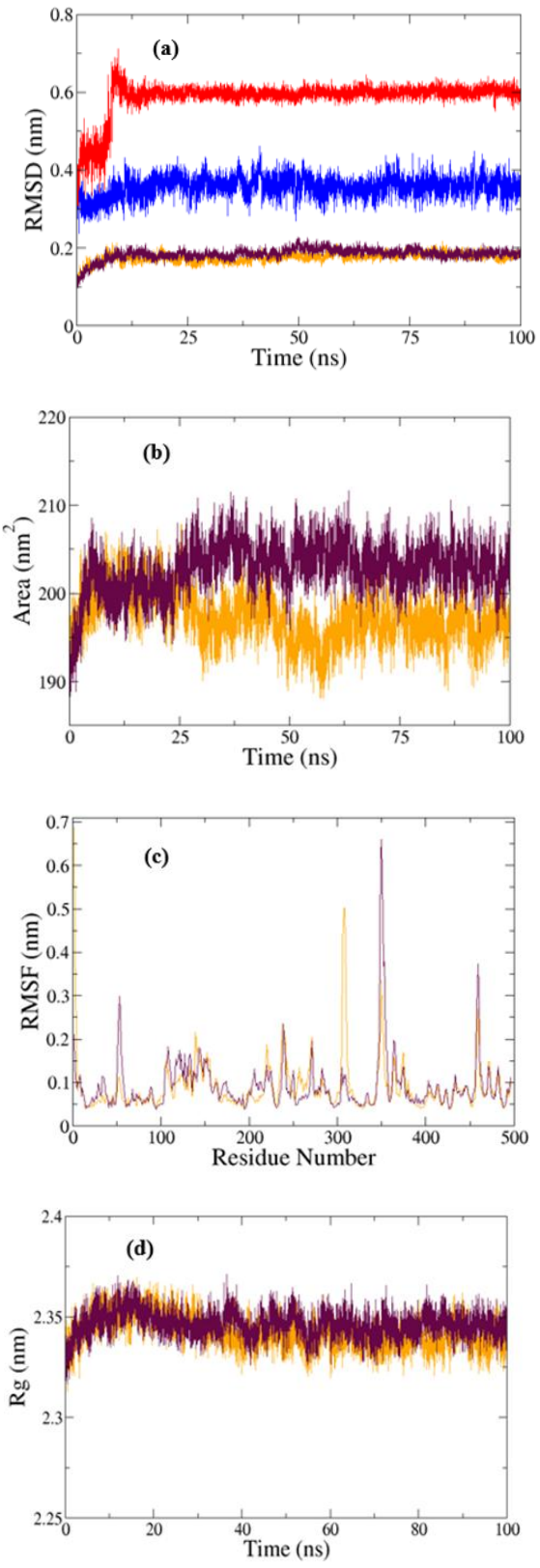

Figure 3. (a) Comparative MDS trajectory with RMSD of **ASC** (red) with protein backbone (maroon) and for **ASD** (blue) with protein backbone (orange), **(b)** SASA of protein in complex with **ASC** (maroon) and **ASD** (orange), **(c)** RMSF plot of protein backbones (maroon-colored curve for **ASC** and orange-colored curve for **ASD** complex) and **(d)** Radius of gyration of protein complexes with ligand **ASC** (maroon) and for **ASD** (orange).
Source: Elaborated by the authors.

3.6.2.4. Solvent accessible surface area (SASA)

The SASA measures the accessible surface of the protein to the solvents quantitatively and the change in compactness of the protein surface on adduct formation with a ligand. The trajectory observed in the SASA plot for each protein complex was regular up to 100 ns with minor fluctuations, as shown in **Fig. 3b**. The value of SASA, the steady areas about 197 and 204 nm^2, was observed for protein-ligand complexes with compounds **ASD** and **ASC**, respectively, suggesting some exposure in protein morphology after adduct formation. The comparison of the SASA of the apo structure (about 200 nm^2) with the complexes of compounds, **ASD** and **ASD**, signified no appreciable change in the SASA, and the value was found even lower for **ASD** complex after adduct formation which was strongly supporting result to interpret the negligible change in the surface area of the enzyme on complex formation and geometrical change in enzyme. The result implied that the change in accessibility of the solvent to the hydrophobic surface of the receptor after binding with the ligand was minimal (Zhang and Lazim, 2017). The apo protein structure MD simulation results are included in the supplementary information (**Fig. 9S**).

3.6.2.5. Hydrogen bond count

The hydrogen bond is a non-covalent interaction that has a significant role in providing stability to the protein-ligand complex in various biological processes (Chikalov *et al.*, 2011). A higher hydrogen bond count would enhance the stability of the complex. **Figure 4** illustrates the variation in hydrogen bond count on the course of MDS between the ligand and protein for 100 ns. Both the ligands (**ASC** and **ASD**) interacted with a high number of hydrogen bonds; **ASC** and **ASD** possess up to 4 or 5 hydrogen bonds most of the time and reach up to 8 hydrogen bonds in some transitions (**Fig. 4**). The result might suggest slightly more stability of the **ASD** complex due to the interaction with protein than the **ASC complex** in different time frames based on hydrogen bond counts.

3.6.2.6. Thermodynamic stability calculations

The binding free energy change (ΔG_{BFE}) from the MMPBSA calculation (**Eqs. 4** and **5**) showed the spontaneity of the complex formation reaction. The total change in binding free energy (ΔG_{BFE}) of the protein-ligand complexes was –138 ± 15 kJ/mol and –91 ± 15 kJ/mol for **ASC** and **ASD** complexes, respectively, as shown in **Table 6**. The equilibrated part of the trajectory of the last 10 ns was taken to calculate the ΔG_{BFE} in complexes.

The van der Waals interaction, polar solvation energy, electrostatic energy, and energy contributions of phases were calculated as energy components using the MMPBSA module. ΔG_{BFE}<0 suggested the spontaneous nature of the complex formation reaction, which could eventually support the active amylase inhibition potential of the ligands (Olsson *et al.*, 2008). The ΔG_{BFE} for the **ASC complex** was found to be quite lower than the ΔGBFE of the ASD complex, which signified the more stable complex formation of the former than the latter. So, the binding affinities, relatively lower RMSD, minimal RMSF, relatively higher hydrogen bond count, and negative ΔG_{BFE} (< –91 kJ/mol) of the protein-ligand complexes could strongly support the HPAE inhibition capability of ligands **ASC** and **ASD.** A figurative presentation of the moving average value of the MMPBSA calculation of free energy change is included in supplementary information (**Fig. 10S**).

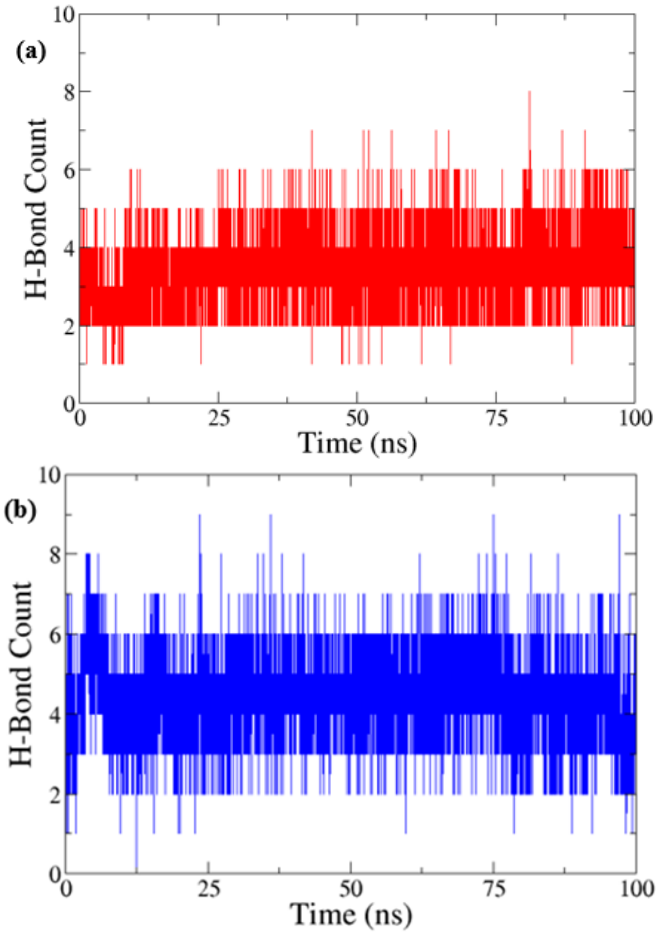

Figure 4. H-bond counts in **(a)** red for the **ASC**-protein complex and **(b)** blue for the **ASD**-protein complex.
Source: Elaborated by the authors.

Table 6. Thermodynamic parameters and their contributions to the total free energy change of complexes.

Binding free energy components	Energy change (kJ/mol) of the receptor with	
	ASC	ASD
ΔV_{DWAALS}	−172 ± 14	−161 ± 14
ΔE_{PB}	252 ± 20	258 ± 23
ΔE_{EL}	−199 ± 22	−170 ± 19
ΔEM_{POLAR}	−18.7 ± 0.6	−18.5 ± 0.6
ΔG_{GAS}	−371 ± 25	−331 ± 15
ΔG_{SOLV}	234 ± 19	241 ± 11
ΔG_{BFE}	**−137 ± 15**	**−91 ± 15**

Note: **ASC** (arborside C); **ASD** (arborside D); value = Energy change ± SD; ΔG_{BFE} = Binding free energy; ΔE_{GAS} = Energy change in gas phase molecular mechanics; ΔE_{ELE} = Electrostatic energy; ΔV_{DWAALS} = van der Waals energy; ΔG_{SOLV} = Electrostatic solvation energy summation; ΔG_{PB} = Polar contributions in solute-solvent system.
Source: Elaborated by the authors.

3.7. Pharmacokinetics and pharmacodynamics of hit candidates

ADMET prediction helps to recognize the significance of ligands towards pharmaceutical efficacy, therapeutic aptitude, pharmacokinetics, and pharmacodynamics (Pires *et al.*, 2015). **Table 7** summarizes the possible results of the ADMET predictions of compounds and drugs. The ligands (**ASC** and **ASD**)

were found in toxicity class 4, indicating a slightly toxic nature (Banerjee *et al.*, 2018). The lethal dose of 50% (LD_{50}) for **ASC** and **ASD** was predicted at 2000 mg/kg, which was lower than that of acarbose, which predicted the toxic nature of the ligand compared to the drug acarbose and less harmful than the drug miglitol (1190 mg/kg). Consensus LogP (<0.6) showed the lipophilicity of both compounds as reference drugs and was comparatively smaller than that of the drugs. None of them followed the Ro5 for drug-likeness except miglitol. Ligand **ASC** was found to be immunotoxic like acarbose, which might indicate the cause of interruption to the immune system (Zerdan *et al.*, 2021). All ligands were inactive regarding hepatotoxicity, carcinogenicity, mutagenicity, cytotoxicity, and phosphoprotein p53. The LD_{50} for **ASC** (2.544 mol/kg) and **ASD** (2.819 mol/kg) were found to be comparable to that of acarbose on oral rat acute toxicity. The logBB value of compounds (< –1) signified poor permeability to the blood-brain barrier (BBB), and the LogSP value (< –4) indicated the impermeability of compounds to the central nervous system (Banerjee *et al.*, 2018; Carpenter *et al.*, 2014). Metabolic properties of both ligands were found, as shown by the drugs. The gastrointestinal absorption factor for the compounds was predicted to be as low as that for drugs, which might depend on the molecular structure and solubility of the candidate. The total clearance measures mainly the hepatic, biliary, and renal clearance, which determines the steady-state dose concentration in the body, and was found to be higher for the compounds than for acarbose and miglitol, which signified that the body could easily release the compound residues through excretion than drugs.

Table 7. ADMET profile of best candidate ligands compared with standard drugs.

ADMET Parameters	Compounds (units)			
	ASC	ASD	*Acarbose	*Miglitol
Toxicity class	4	4	6	4
LD_{50} (mg/kg)	2000	2000	24000	1190
Lipinski rule (RO5)	No	No	No	yes
Consensus LogP	−0.31	−1.12	−6.22	−3.26
Immunotoxicity	Active	Inactive	Active	Active
Hepatotoxicity	Inactive	Inactive	Inactive	Active
Carcinogenicity	Inactive	Inactive	Inactive	Inactive
Mutagenicity	Inactive	Inactive	Inactive	Inactive
Cytotoxicity	Inactive	Inactive	Inactive	Inactive
Phosphoprotein p53	Inactive	Inactive	Inactive	Inactive
CYP2D6 substrate	No	No	No	No
CYP3A4 substrate	No	No	No	No
CYP2C9 inhibitor	No	No	No	No
CYP2C19 inhibitor	No	No	No	No
CYP2D6 inhibitor	No	No	No	No
CYP3A4 inhibitor	No	No	No	No
Oral rat acute toxicity (mol/kg)	2.544	2.819	2.447	2.257
BBB permeability (logBB)	−1.456	−1.496	−1.717	−1.501
CNS permeability (logPS)	−4.27	−4.517	−6.438	−4.842
GI absorption	Low	Low	Low	Low
Total clearance log (mL/min/kg)	1.009	1.031	0.428	0.815

Note: **ASC** (Arborside C), **ASD** (Arborside D), and *Reference drugs.
Source: Elaborated by the authors.

The comparison of top candidates with the standard drugs acarbose and miglitol (Basnet *et al.*, 2023) implied the positive therapeutic behavior of compounds. Hence, the ADMET analysis of the compounds **ASC** and **ASD** revealed comparative therapeutic significance to the standard drugs.

Plant *N. arbor-tristis* has been reported on various biological activities like antioxidant, antidiabetic, and cytotoxicity in different methodologies to expose its medicinal significance. However, six different solvent extracts of leaves of *N. arbor-tristis* through sequential extraction in ascending polarity and their ethnomedicinal studies through *in vitro* and computational antidiabetic analysis using HPAE in detail have not been carried out yet.

This study showed the presence of different phytochemicals containing alkaloids, flavonoids, phenolic compounds, glycosides, and reducing sugars in the leaves of the selected plant. Quantitative phytochemical analysis revealed the presence of high phenolic contents in the acetone extract (**AE**) and methanolic extract (**ME**) of 137 ± 4 mg GAE/g and 139 ± 4 mg GAE/g, respectively (**Table 3**). Chloroform extract (**CE**) and hexane extract (**HE**) were found to have high TFC compared to other extract fractions.

The result portrayed the significant antioxidant nature of the leaf extract of *N. arbor-tristis,* as extract **ME** showed the best antioxidant activity with an IC_{50} of 56 ± 3 µg/mL among all leaf extracts, which was comparable to the antioxidant activity of the control ascorbic acid. Other extracts showed moderate antioxidizing potential toward DPPH free radicals. Akki *et al.* (2009) studied the DPPH scavenging assay of plant leaves in different solvents (pet ether, butanol, ethyl acetate, and butylated hydroxytoluene), and butanol extract showed the best scavenging against DPPH radical. Formerly, the medicinal properties of this plant have been explored in the flowers and seeds of the plant and found to have significant antioxidant properties of different extracts (Mishra *et al.*, 2016; Mishra *et al.*, 2022). The therapeutic potential of natural products is due to the presence of phytoconstituents containing iridoids, flavonoids, alkaloids, and others (Chauhan and Banerjee, 2024; Naseem *et al.*, 2024). The quantitative phytochemical assessment showed the presence of high phenolic content in extracts **AE** and **ME**, and similarly high flavonoid content in all extracts except **DWE**. A better antioxidant nature of **ME** might be due to the presence of functional components than in other extracts. These could act upon harmful reactive oxygen, reactive nitrogen, and free radical species in the human body to minimize alternation in cellular functioning,

metabolism, and could prevent the formation of diseases (Yang *et al.*, 2016). A high content of metabolites containing flavonoids, phenolics, and iridoids in extracts is the backbone of their pharmaceutical significance, which has supported the observations of this study (Phuyal *et al.*, 2020).

In this study, extract **HE** was found to be most lethal to *Artemia salina* nauplii, and the lethal concentration of 97 ± 2 µg/mL in BSLA. The toxicity of the extracts, **ME** and **CE**, was found to be comparable to that of **HE**, and other extracts were found to be less toxic than the control potassium dichromate (**Table 4**). The results showed that **HE**, **ME**, and **EAE** were found (LC_{50} < 200 µg/mL) moderately toxic, other extracts (LC_{50} < 500 µg/mL) were found weakly toxic, and **DWE** (LC_{50} > 500 µg/mL) was found nontoxic (Niksic *et al.*, 2021). The BSLA assay helps to evaluate the potential of herbal plants towards anticancer activity through cytotoxicity screening (Meyer *et al.*, 1982).

The α-amylase inhibition assay helped estimate the potential antidiabetic activity of the different leaf extract fractions. A computational approach using human pancreatic amylase enzyme was carried out to analyze the possible effective interactions, the molecular mechanism of complex formation, and to support the *in vitro* antidiabetic activity. Methanolic extract fraction (**ME**) was the most potent amylase inhibitor with IC_{50}, 157 ± 3 µg/mL compared to other fractions and standard acarbose (**Table 4**). Extract **HE** and **CE** showed mild inhibition activity, and the rest of the fractions showed weak inhibition activity against *α*-amylase. A computational examination of compounds found in leaves of *N. arbor-tristis* (**Table 1**) was carried out. The *in vitro* experimental outcome and computational results helped to better understand the molecular mechanism and possible effective interaction of the ligand with the target protein. To predict the possible compound responsible for amylase inhibition, previously isolated and reported compounds of *N. arbor-tristis* characterized by GC-MS, LC-MS, ^{1}H NMR, and ^{13}C NMR were selected. Such structures were optimized, energy minimized, and screened through molecular docking and MDS. Among all the selected compounds, **ASC** and **ASD** were found to be bound most effectively to the amylase enzyme, which could be proposed as potential HPAE inhibitors, as interpreted by molecular docking calculation with a high binding affinity (–33.5 kJ/mol for both), reasonable geometric configuration, and thermodynamic parameters. Negative binding free energy (ΔG_{BFE} < 0), comparative pharmacokinetic and pharmacodynamic properties of the compounds compared with the drugs Acarbose and Miglitol (**Table 7**), shown by ADMET profiling, provided strong evidence of spontaneity of the complexes along with binding efficacy to HPAE and drug likeness through computer-based assessments. The amylase inhibition potential of the extracts and stability of the enzyme-ligand complexes on computational screening portrayed the extracts' HPAE inhibition capability and the plant's antidiabetic potential.

Overall, the results of this study illustrated and supported the ethnomedicinal importance of the leaf extract of *N. arbor-tristis*. The high content of potential bioactive metabolites, *in vitro* experiments, and computational virtual screening outputs supported the good antioxidant and HPAE inhibition potential of the plant.

4. Conclusions

The study showed that the methanolic extract (**ME**) was found to be the most significant extract in all *in vitro* antioxidants, *α*-amylase inhibition, and brine shrimp lethality assays; however, other fractions showed moderate responses to the bioactivity evaluations. Among the selected ligands, arborside-C (**ASC**) and arborside-D (**ASD**) showed significant affinity to the human pancreatic α-amylase enzyme, as determined through molecular docking, molecular dynamics simulation, and ADMET profiling. Polar regions of the ligands (mainly the hydroxyl group) were found to be effective binding sites to the target protein amylase in molecular docking analysis. The integration of *in vitro* and *in silico* analysis in this study demonstrated the potential amylase inhibitory capability of plant phytoconstituents. As *in silico* analysis gives the possible therapeutic estimation through virtual screening at a molecular level, the phytochemicals isolated from this plant (hit candidates arborside-C, and arborside-D) were proposed to be used for *in vivo* bio-characterization, validation, and optimization to estimate their medicinal significance to treat hyperglycemia through the amylase enzyme inhibition mechanism.

Authors' contribution

Conceptualization: Ram Lal Swagat Shrestha; Jhashanath Adhikari Subin; Bishnu Prasad Marasini; **Data curation**: Jhashanath Adhikari Subin; Nirmal Parajuli; Prabhat Neupane; **Formal Analysis**: Jhashanath Adhikari Subin; Bishnu Prasad Marasini; Nirmal Parajuli; **Funding acquisition**: Ram Lal Swagat Shrestha; Nirmal Parajuli; Timila Shrestha; **Investigation**: Jhashanath Adhikari Subin; Bishnu Prasad Marasini; **Methodology**: Ram Lal Swagat Shrestha; Jhashanath Adhikari Subin; Bishnu Prasad Marasini; **Project administration**: Ram Lal Swagat Shrestha; Timila Shrestha; **Resources**: Ram Lal Swagat Shrestha; Binita Maharjan; Samjhana Bharati; **Software**: Ram Lal Swagat Shrestha; Jhashanath Adhikari Subin; **Supervision**: Ram Lal Swagat Shrestha; Jhashanath Adhikari Subin; Bishnu Prasad Marasini; **Validation**: Jhashanath Adhikari Subin; Bishnu Prasad Marasini; Nirmal Parajuli; **Visualization**: Nirmal Parajuli; Prabhat Neupane; Sujan Dhital; Samjhana Bharati; **Writing – original draft**: Nirmal Parajuli; **Writing – review & editing**: Jhashanath Adhikari Subin; Bishnu Prasad Marasini; Binita Maharjan; Nirmal Parajuli.

Data availability statement

The data will be available upon request from the main and corresponding authors.

Funding

Not applicable.

Acknowledgments

The authors express gratitude to the Amrit Science Campus, Tribhuvan University, and Kathmandu Valley College for laboratory facilities for extraction and computation.

Conflict of interest

The authors declare that there is no conflict of interest.

References

Abraham, M. J.; Murtola, T.; Schulz, R.; Páll, S.; Smith, J. C.; Hess, B.; Lindah, E. Gromacs: High Performance Molecular Simulations through Multi-Level Parallelism from Laptops to Supercomputers. *SoftwareX*. **2015**, *1* (2), 19–25. https://doi.org/10.1016/j.softx.2015.06.001

Adcock, S. A.; McCammon, J. A. Molecular Dynamics: Survey of Methods for Simulating the Activity of Proteins. *Chem. Rev.* **2006**, *106*, 1589–1615. https://doi.org/10.1021/cr040426m

Agrawal, J.; Pal, A. *Nyctanthes arbor-tristis* Linn - A Critical Ethnopharmacological Review. *J. Ethnopharmacol.* **2013**, *146*, 645–658. https://doi.org/10.1016/j.jep.2013.01.024

Ahmed, S.; Ali, M. C.; Ruma, R. A.; Mahmud, S.; Paul, G. K.; Saleh, M. A.; Alshahrani, M. M.; Obaidullah, A. J.; Biswas, S. K.; Rahman, M. M.; Rahman, M. M.; Islam, M. R. Molecular Docking and Dynamics Simulation of Natural Compounds from Betel Leaves (*Piper Betle* L.) for Investigating the Potential Inhibition of Alpha-Amylase and Alpha-Glucosidase of Type 2 Diabetes. *Molecules*. **2022**, *27* (14), 4526. https://doi.org/10.3390/molecules27144526

Aier, I.; Varadwaj, P. K.; Raj, U. Structural Insights into Conformational Stability of Both Wild-Type and Mutant EZH2 Receptor. *Sci. Rep*. **2016**, *6* (1), 34984. https://doi.org/10.1038/srep34984

Akki, K. S.; Krishnamurthy, G.; Bhoja Naik, H. S. Phytochemical Investigations and *in vitro* Evaluation of *Nyctanthes arbor-tristis* Leaf Extracts for Antioxidant Property. *J. Pharm. Res.* **2009**, *2* (4), 752–755.

Banerjee, P.; Eckert, A. O.; Schrey, A. K.; Preissner, R. ProTox-II: A Webserver for the Prediction of Toxicity of Chemicals. *Nucleic Acids Res*. **2018**, *46* (1), 257–263. https://doi.org/10.1093/nar/gky318

Banu, K. S.; Cathrine, L. General Techniques Involved in Phytochemical Analysis. *Int. J. Adv. Res. Chem. Sci.* **2015**, *2* (4), 25–32.

Basnet, S.; Ghimire, M. P.; Lamichhane, T. R.; Adhikari, R.; Adhikari, A. Identification of Potential Human Pancreatic Aamylase Inhibitors from Natural Products by Molecular Docking, MM/GBSA Calculations, MD Simulations, and ADMET Analysis. *PLoS One*. **2023**, *18*, 1–13. https://doi.org/10.1371/journal.pone.0275765

Bb, C.; Pandeya, S.; Kp, G.; Bharati L Phytochemical Screening and Cytotoxic Activity of *Nyctanthes arbor tristis*. *Indian Res. J. Pharm. Sci.* **2015**, *2* (2), 205–217.

Berman, H. M.; Westbrook, J.; Feng, Z.; Gilliland, G.; Bhat, T. N.; Weissig, H.; Shindyalov, I. N.; Bourne, P. E. The Protein Data Bank. *Nucleic Acids Res.* **2000**, *28* (1), 235-242. https://doi.org/10.1093/nar/28.1.235

Bitew, M.; Desalegn, T.; Demissie, T. B.; Belayneh, A.; Endale, M.; Eswaramoorthy, R. Pharmacokinetics and Drug-Likeness of Antidiabetic Flavonoids: Molecular Docking and DFT Study. *PLoS One*. **2021**, *16*, 0260853. https://doi.org/10.1371/journal.pone.0260853

Blois, M. S. Antioxidant Determinations by the Use of a Stable Free Radical. *Nature*. **1958**, *181* (4617), 1199–1200. https://doi.org/10.1038/1811199a0

Butler, M. S. The Role of Natural Product Chemistry in Drug Discovery. *J. Nat. Prod.* **2004**, *67*, 2141–2153. https://doi.org/10.1021/np040106y

Carpenter, T. S.; Kirshner, D. A.; Lau, E. Y.; Wong, S. E.; Nilmeier, J. P.; Lightstone, F. C. A Method to Predict Blood-Brain Barrier Permeability of Drug-Like Compounds Using Molecular Dynamics Simulations. *Biophys J*. **2014**, *107* (3), 630–641. https://doi.org/10.1016/j.bpj.2014.06.024

Cele, N.; Awolade, P.; Seboletswe, P.; Olofinsan, K.; Islam, M. S.; Singh, P. α-Glucosidase and α-Amylase Inhibitory Potentials of Quinoline–1,3,4-Oxadiazole Conjugates Bearing 1,2,3-Triazole with Antioxidant Activity, Kinetic Studies, and Computational Validation. *Pharmaceuticals*. **2022**, *15* (8), 1035. https://doi.org/10.3390/ph15081035

Chandra, S.; Khan, S.; Avula, B.; Lata, H.; Yang, M. H.; Elsohly, M. A.; Khan, I. A. Assessment of Total Phenolic and Flavonoid Content, Antioxidant Properties, and Yield of Aeroponically and Conventionally Grown Leafy Vegetables and Fruit Crops: A Comparative Study. *Evidence-Based Complement Alternat Med.* **2014**, *2014*, 253875. https://doi.org/10.1155/2014/253875

Chauhan, A.; Banerjee, R. Evaluation of Traditional Uses, Phytochemical Constituents, Therapeutic Uses and Future Prospects of *pyracantha* Genus: A Systematic Review. *Nat. Prod. Res*. **2024**, *39* (5) 922–934. https://doi.org/10.1080/14786419.2024.2319660

Chikalov, I.; Yao, P.; Moshkov, M.; Latombe, J. C. Learning Probabilistic Models of Hydrogen Bond Stability from Molecular Dynamics Simulation Trajectories. *BMC Bioinformatics*. **2011**, *12* (SUPPL. 1), 1–6. https://doi.org/10.1186/1471-2105-12-S1-S34

Choo, M. Z. Y.; Chai, C. L. L. The Polypharmacology of Natural Products in Drug Discovery and Development. *Annu. Rep. Med. Chem.* **2023**, *61*, 55–100. https://doi.org/10.1016/bs.armc.2023.10.002

Chothani, S. R.; Dholariya, M. P.; Joshi, R. J.; Chamakiya, C. A.; Maliwal, D.; Pissurlenkar, R. R. S.; Patel, A. S.; Bhalodia, J. J.; Ambasana, M. A.; Patel, R. B.; Bapodra, A. H.; Kapuriya, N. P. Solvent-Free Synthesis, Biological Evaluation and *in silico* Studies of Novel 2-Amino-7-(Bis(2-Hydroxyethyl)Amino)-4H-Chromene-3-Carbonitrile Derivatives as Potential a-Amylase Inhibitors. *J. Mol. Struct*. **2024**, *1301*, 137462. https://doi.org/10.1016/j.molstruc.2023.137462

Das, A. P.; Mathur, P.; Agarwal, S. M. Machine Learning, Molecular Docking, and Dynamics-Based Computational Identification of Potential Inhibitors against Lung Cancer. *ACS Omega*. **2024**, *9* (4), 4528–4539. https://doi.org/10.1021/acsomega.3c07338

Dewi, N. K. S. M.; Fakhrudin, N.; Wahyuono, S. A Comprehensive Review on the Phytoconstituents and Biological Activities of *Nyctanthes arbor-tristis* L. *J. Appl. Pharm. Sci*. **2022**, *12* (8), 9–17. https://doi.org/10.7324/JAPS.2022.120802

Gautam, V. S.; Singh, A.; Kumari, P.; Nishad, J. H.; Kumar, J.; Yadav, M.; Bharti, R.; Prajapati, P.; Kharwar, R. N. Phenolic and Flavonoid Contents and Antioxidant Activity of an Endophytic Fungus *Nigrospora sphaerica* (EHL2), Inhabiting the Medicinal Plant *Euphorbia Hirta* (Dudhi) L. *Arch. Microbiol*. **2022**, *204* (140), 1–13. https://doi.org/10.1007/s00203-021-02650-7

Hanwell, M. D.; Curtis, D. E.; Lonie, D. C.; Vandermeerschd, T.; Zurek, E.; Hutchison, G. R. Avogadro: An Advanced Semantic Chemical Editor, Visualization, and Analysis Platform. *J. Cheminform*. **2012**, *4* (8), 1–13. https://doi.org/10.1186/1758-2946-4-17

Hollingsworth, S. A.; Dror, R. O. Molecular Dynamics Simulation for All. *Neuron 99*. **2018**, *6*, 1129–1143. https://doi.org/10.1016/j.neuron.2018.08.011

Jain, P. K.; Pandey, A. The Wonder of Ayurvedic Medicine-*Nyctanthes arbor-tristis*. *Int. J. Herb. Med*. **2016**, *9* (4), 9–17.

Khakurel, D.; Uprety, Y.; Ahn, G.; Cha, J. Y.; Kim, W. Y.; Lee, S. H.; Rajbhandary, S. Diversity, Distribution, and Sustainability of Traditional Medicinal Plants in Kaski District, Western Nepal. *Front Pharmacol*. **2022**, *13,* 1076351. https://doi.org/10.3389/fphar.2022.1076351

Kumar, S.; Saini, R.; Suthar, P.; Kumar, V.; Sharma, R. Plant Secondary Metabolites: Their Food and Therapeutic Importance. *Plant Secondary Metabolites*; Springer, Singapore, **2022**, 371–2022. https://doi.org/10.1007/978-981-16-4779-6_12

Kunwar, R. M.; Baral, K.; Paudel, P.; Acharya, R. P.; Thapa-Magar, K. B.; Cameron, M.; Bussmann, R. W. Land-Use and Socioeconomic Change, Medicinal Plant Selection and Biodiversity Resilience in Far Western Nepal. *PLoS One*. **2016**, *11* (12), 0167812. https://doi.org/10.1371/journal.pone.0167812

Kushwah, P.; Jain, G.; Patidar, A.; Baghel, J. S.; Agarwal, A. From Ancient Remedies to Modern Marvels: Unveiling the Medicinal Secrets of *Nyctanthes arbor-tristis* and *Piper Betle* Linn. Leaves- A Comprehensive Review. *Int. J. Pharm. Sci. Med*. **2023**, *8* (12), 11–24. https://doi.org/10.47760/ijpsm.2023.v08i12.002

Laware, S. G.; Shirole, N. L. Formulation and Development of Polyherbal Ointment Containing *Clerodendrum Serratum, Solanum Xanthocarpum,* and *Nyctanthes Arbort ristis* Extracts and Assessment of Anti-Inflammatory

Activity in Carrageenan-Induced Paw Edema Model. *Int. J. Pharm. Qual. Assur.* **2023**, *14* (3), 523–528. https://doi.org/10.25258/ijpqa.14.3.10

Liu, M.; Hu, B.; Zhang, H.; Zhang, Y.; Wang, L.; Qian, H.; Qi, X. Inhibition Study of Red Rice Polyphenols on Pancreatic α-Amylase Activity by Kinetic Analysis and Molecular Docking. *J. Cereal Sci*. **2017A**, *76*, 186–192. https://doi.org/10.1016/j.jcs.2017.04.011

Liu, P.; Lu, J.; Yu, H.; Ren, N.; Lockwood, F. E.; Wang, Q. J. Lubricant Shear Thinning Behavior Correlated with Variation of Radius of Gyration *via* Molecular Dynamics Simulations. *J. Chem. Phys*. **2017B**, *147* (8), 084904. https://doi.org/10.1063/1.4986552

Lolok, N.; Sumiwi, S. A.; Muhtadi, A.; Susilawati, Y.; Hendriani, R.; Ramadhan, D. S. F.; Levita, J.; Sahidin, I. Molecular Docking and Molecular Dynamics Studies of Bioactive Compounds Contained in Noni Fruit (*Morinda citrifolia* L.) against Human Pancreatic α-Amylase. *J. Biomol. Struct. Dyn*. **2022**, *40* (15), 7091–7098. https://doi.org/10.1080/07391102.2021.1894981

Majumder, R.; Adhikari, L.; Hossain, C. M.; Dhara, M.; Sahu, J. Toxicological Evaluation, Brine Shrimp Lethality Assay, *in vivo* and *ex vivo* Antioxidant Assessment Followed by GC-MS Study of the Extracts Obtained from *Olax Psittacorum* (Lam.) Vahl. *Orient. Pharm. Exp. Med*. **2019**, 1–23. https://doi.org/10.1007/s13596-019-00384-y

Martínez, L. Automatic Identification of Mobile and Rigid Substructures in Molecular Dynamics Simulations and Fractional Structural Fluctuation Analysis. *PLoS One*. **2015**, *10* (3), 0119264. https://doi.org/10.1371/journal.pone.0119264

Meshram, M. M.; Rangari, S. B.; Kshirsagar, S. B.; Gajbhiye, S.; Trivedi, M. R.; Sahane, R. S. *Nyctanthes arbor-tristis* a Herbal Panacea. *IJPSR*. **2012**, *3* (8), 2432–2440.

Meyer, B. N.; Ferrigni, N. A.; Putnam, J. E.; Jacobsen, L. B.; Nichols, D. E.; Mclaughlin, J. L. Brine Shrimp: A Convenient General Bioassay for Active Plant Constituents. *J. Med. Plants. Res*. **1982**, *45*, 31–34. https://doi.org/10.1055/s-2007-971236

Mishra, A. K.; Tiwari, K. N.; Saini, R.; Chaurasia, J. K.; Mishra, S. K. Assessment of Antioxidant Potential in Seed Extracts of *Nyctanthes arbor-tristis* L. and Phytochemical Profiling by Gas Chromatography-Mass Spectrometry System. *Braz. J. Pharm. Sci.*, **2022**, *58*, e21180. https://doi.org/10.1590/s2175-97902022e21180

Mishra, A. K.; Upadhyay, R.; Chaurasia, J. K.; Tiwari, K. N. Comparative Antioxidant Study in Different Flower Extracts of *Nyctanthes arbor-tristis* (L.) (Oleaceae): an Important Medicinal Plant. *Braz. J. Bot.*, **2016**, *39*, 813–820. https://doi.org/10.1007/s40415-016-0283-x

Mohamed, G. A.; Omar, A. M.; El-Araby, M. E.; Mass, S.; Ibrahim, S. R. M. Assessments of Alpha-Amylase Inhibitory Potential of Tagetes Flavonoids through *in vitro*, Molecular Docking, and Molecular Dynamics Simulation Studies. *Int. J. Mol. Sci*. **2023**, *24* (12), 10195. https://doi.org/10.3390/ijms241210195

Mustafa, I.; Faisal, M. N.; Hussain, G.; Muzaffar, H.; Imran, M.; Ijaz, M. U.; Sohail, M. U.; Iftikhar, A.; Shaukat, A.; Anwar, H. Efficacy of Euphorbia Helioscopia in Context to a Possible Connection between Antioxidant and Antidiabetic Activities: A Comparative Study of Different Extracts. *BMC Complement Med Ther*. **2021**, *21* (1), 1–12. https://doi.org/10.1186/s12906-021-03237-x

Naseem, N.; Khaliq, T.; Jan, S.; Nabi, S.; Sultan, P.; Hassan, Q. P.; Mir, F. A. An Overview on Pharmacological Significance, Phytochemical Potential, Traditional Importance and Conservation Strategies of *Dioscorea deltoidea*: A High Valued Endangered Medicinal Plant. *Heliyon*. **2024**, *10* (10), e31245. https://doi.org/10.1016/j.heliyon.2024.e31245

Niksic, H.; Becic, F.; Koric, E.; Gusic, I.; Omeragic, E.; Muratovic, S.; Miladinovic, B.; Duric, K. Cytotoxicity Screening of Thymus Vulgaris L. Essential Oil in Brine Shrimp Nauplii and Cancer Cell Lines. *Sci Rep*. **2021**, *11* (13178), 1–9. https://doi.org/10.1038/s41598-021-92679-x

Ogunyemi, O. M.; Gyebi, G. A.; Saheed, A.; Paul, J.; Nwaneri-Chidozie, V.; Olorundare, O.; Adebayo, J.; Koketsu, M.; Aljarba, N.; Alkahtani, S.; Batiha, G. E. S.; Olaiya, C. O. Inhibition Mechanism of Alpha-Amylase, a Diabetes Target, by a Steroidal Pregnane and Pregnane Glycosides Derived from *Gongronema latifolium* Benth. *Front. Mol. Biosci*. **2022**, *9*, 866719. https://doi.org/10.3389/fmolb.2022.866719

Olsson, T. S. G.; Williams, M. A.; Pitt, W. R.; Ladbury, J. E. The Thermodynamics of Protein-Ligand Interaction and Solvation: Insights for Ligand Design. *J. Mol. Biol*. **2008**, *384* (4), 1002–1017. https://doi.org/10.1016/j.jmb.2008.09.073

Omar, A. M.; AlKharboush, D. F.; Mohammad, K. A.; Mohamed, G. A.; Abdallah, H. M.; Ibrahim, S. R. M. Mangosteen Metabolites as Promising Alpha-Amylase Inhibitor Candidates: *In silico* and *in vitro* Evaluations. *Metabolites*. **2022**, *12* (12), 1239. https://doi.org/10.3390/metabo12121229

Onufriev, A. V; Case, D. A. Generalized Born Implicit Solvent Models for Biomolecules. *Annu. Rev. Biophys.* **2019**, *48* (1), 275–298. https://doi.org/10.1146/annurev-biophys-052118-115325

Phuyal, N.; Jha, P. K.; Raturi, P. P.; Rajbhandary, S. Total Phenolic, Flavonoid Contents, and Antioxidant Activities of Fruit, Seed, and Bark Extracts of *Zanthoxylum armatum* DC. *Sci. World J*. **2020**, *2020,* 8780704. https://doi.org/10.1155/2020/8780704

Pires, D. E. V.; Blundell, T. L.; Ascher, D. B. PkCSM: Predicting Small-Molecule Pharmacokinetic and Toxicity Properties Using Graph-Based Signatures. *J. Med. Chem*. **2015**, *58* (9), 4066–4072. https://doi.org/10.1021/acs.jmedchem.5b00104

Proença, C.; Freitas, M.; Ribeiro, D.; Tomé, S. M.; Oliveira, E. F. T.; Viegas, M. F.; Araújo, A. N.; Ramos, M. J.; Silva, A. M. S.; Fernandes, P. A.; Fernandes, E. Evaluation of a Flavonoids Library for Inhibition of Pancreatic α-Amylase towards a Structure–Activity Relationship. *J. Enzyme Inhib. Med. Chem*. **2019**, *34* (1), 577–588. https://doi.org/10.1080/14756366.2018.1558221

Rathore, A.; Juneja, R. K.; Tandon, J. S. An Iridoid Glucoside Form *Nyctanthes arbor-tristis*. *Phytochemistry*. **1989**, *28* (7), 1913–1917. https://doi.org/10.1016/S0031-9422(00)97886-5

Rawat, H.; Verma, Y.; Saini, N.; Negi, N.; Pant, H. C.; Mishra, A. *Nyctanthes arbor-tristis*: A Traditional Herbal Plant with Miraculous Potential in Medicine. *Int. J. Bot. Stud*. **2021**, *6* (3), 427–440.

Renganathan, S.; Manokaran, S.; Vasanthakumar, P.; Singaravelu, U.; Kim, P. S.; Kutzner, A.; Heese, K. Phytochemical Profiling in Conjunction with *in vitro* and *in silico* Studies to Identify Human α-Amylase Inhibitors in *Leucaena leucocephala* (Lam.) de Wit for the Treatment of Diabetes Mellitus. *ACS Omega*. **2021**, *6* (29), 19045–19057. https://doi.org/10.1021/acsomega.1c02350

Sabudak, T.; Demirkiran, O.; Ozturk, M.; Topcu, G. Phenolic Compounds from *Trifolium echinatum* Bieb. and Investigation of Their Tyrosinase Inhibitory and Antioxidant Activities. *Phytochemistry*. **2013**, *96*, 305–311. https://doi.org/10.1016/j.phytochem.2013.08.014

Sah, A. K.; Verma, V. K. Phytochemicals and Pharmacological Potential of *Nyctanthes arbor-tristis*: A Comprehensive Review. *Int. J. Res. Pharm. Biomed. Sci.* **2012**, *3* (1), 420–427.

Sethi, S.; Joshi, A.; Arora, B.; Bhowmik, A.; Sharma, R. R.; Kumar, P. Significance of FRAP, DPPH, and CUPRAC Assays for Antioxidant Activity Determination in Apple Fruit Extracts. *Eur. Food Res. Technol*. **2020**, *246* (3), 591–598. https://doi.org/10.1007/s00217-020-03432-z

Shaweta, S.; Akhil, S.; Utsav, G. Molecular Docking Studies on the Anti-Fungal Activity of Allium Sativum (Garlic) against Mucormycosis (Black Fungus) by BIOVIA Discovery Studio Visualizer 21.1.0.0. *Ann. Antivir Antiretrovir*. **2021**, *5* (1), 28–32. https://doi.org/https://doi.org/10.21203/rs.3.rs-888192/v1

Shrestha, T.; Maharjan, B.; Panta, R.; Lal Swagat Shrestha, R.; Parajuli, N.; Neupane, P.; Dhital, S.; Bharati, S.; Adhikari Subin, J.; Marasini, P. Molecular Docking and ADMET Prediction of Compounds from *Piper Longum* L. Detected by GC-MS Analysis in Diabetes Management. *Mor. J. Chem*. **2024**, *2024* (2), 776–798. https://doi.org/10.48317/IMIST.PRSM/morjchem-v12i2.46845

Solanki, M.; Rajhans, S.; Pandya, H. A.; Mankad, A. U. *Nyctanthes arbor-tristis* Linn: A Short Review. *World J. Pharm. Pharm. Sci*. **2021**, *10* (3), 1047–1054. https://doi.org/10.20959/wjpps20213-18575

Stănciuc, N.; Râpeanu, G.; Bahrim, G. E.; Aprodu, I. The Interaction of Bovine β-Lactoglobulin with Caffeic Acid: From Binding Mechanisms to Functional Complexes. *Biomolecules*. **2020**, *10* (8), 1–14. https://doi.org/10.3390/biom10081096

Sugandh, F.; Chandio, M.; Raveena, F.; Kumar, L.; Karishma, F.; Khuwaja, S.; Memon, U. A.; Bai, K.; Kashif, M.; Varrassi, G.; Khatri, M.; Kumar, S. Advances in the Management of Diabetes Mellitus: A Focus on Personalized Medicine. *Cureus*. **2023**, *15* (8), e43697. https://doi.org/10.7759/cureus.43697

Trott, O.; Olson, A. J. AutoDock Vina: Improving the Speed and Accuracy of Docking with a New Scoring Function, Efficient Optimization, and Multithreading. *J. Comput. Chem*. **2009**, *31*, 455-461. https://doi.org/10.1002/jcc.21334

Vasanthkumar, J.; Hulikal, A.; Santoshkumar, S.; Sripathy, H. *In silico* Docking Studies of α - Amylase Inhibitors from the Anti - Diabetic Plant *Leucas ciliata* Benth and an Endophyte, *Streptomyces longisporoflavus*. *3 Biotech*. **2021**, *11* (2), 1–16. https://doi.org/10.1007/s13205-020-02547-0

Vishwakarma, R. K.; Negi, A.; Negi, D. S. Abortitristoside A and Desrhamnosylverbanscoside: The Potential COX-2 Inhibitor from the Leaves of *Nyctanthes arbor-tristis* as Anti-Inammatory Agents Based on the *in vitro* Assay, Molecular Docking and ADMET Prediction. *Chem. Pap.* **2022**, *77* (6), 3035-3049. https://doi.org/10.21203/rs.3.rs-1345800/v2

Wang, E.; Sun, H.; Wang, J.; Wang, Z.; Liu, H.; Zhang, J. Z. H.; Hou, T. End-Point Binding Free Energy Calculation with MM/PBSA and MM/GBSA: Strategies and Applications in Drug Design. *Chem. Rev.* **2019**, *119*, 9478–9508. https://doi.org/10.1021/acs.chemrev.9b00055

Yang, Y.; Karakhanova, S.; Hartwig, W.; D'Haese, J. G.; Philippov, P. P.; Werner, J.; Bazhin, A. V. Mitochondria and Mitochondrial ROS in Cancer: Novel Targets for Anticancer Therapy. *J. Cell Physiol*. **2016**, *231* (12), 2570–2581. https://doi.org/10.1002/jcp.25349

Yi, J.; Zhao, T.; Zhang, Y.; Tan, Y.; Han, X.; Tang, Y.; Chen, G. Isolated Compounds from Dracaena Angustifolia Roxb and Acarbose Synergistically/Additively Inhibit α-Glucosidase and α-Amylase: An *in vitro* Study. *BMC Complement Med Ther*. **2022**, *22* (177), 1–12. https://doi.org/10.1186/s12906-022-03649-3

Yuan, S.; Chan, H. C. S.; Hu, Z. Using PyMOL as a Platform for Computational Drug Design. *Wiley Interdiscip. Rev. Comput. Mol. Sci.* **2017**, *7*, 1298. https://doi.org/10.1002/wcms.1298

Zahra, S.; Zaib, S.; Khan, I. Identification of Isobenzofuranone Derivatives as Promising Antidiabetic Agents: Synthesis, *in vitro* and *in vivo* Inhibition of α-Glucosidase and α-Amylase, Computational Docking Analysis and Molecular Dynamics Simulations. *Int. J. Biol. Macromol*. **2024**, *259* (2), 129241. https://doi.org/10.1016/j.ijbiomac.2024.129241

Zain, S. N. D. M.; Omar, W. A. W. Antioxidant Activity, Total Phenolic Content and Total Flavonoid Content of Water and Methanol Extracts of *Phyllanthus* Species from Malaysia. *Pharmacogn J*. **2018**, *10* (4), 677–681. https://doi.org/10.5530/pj.2018.4.111

Zerdan, M. B.; Moussa, S.; Atoui, A.; Assi, H. I. Mechanisms of Immunotoxicity: Stressors and Evaluators. *Int. J. Mol. Sci.* **2021**, *22* (15), 8242. https://doi.org/10.3390/ijms22158242

Zhang, D.; Lazim, R. Application of Conventional Molecular Dynamics Simulation in Evaluating the Stability of Apomyoglobin in Urea Solution. *Sci. Rep*. **2017**, *7,* 44651. https://doi.org/10.1038/srep44651

Zhao, Y.; Wang, M.; Huang, G. Structure-Activity Relationship and Interaction Mechanism of Nine Structurally Similar Flavonoids and α-Amylase. *J. Funct. Foods*. **2021**, *86*, 104739. https://doi.org/10.1016/j.jff.2021.104739

Zoete, V.; Cuendet, M. A.; Grosdidier, A.; Michielin, O. SwissParam: A Fast Force Field Generation Tool for Small Organic Molecules. *J. Comput. Chem*. **2011**, *32* (11), 2359–2368. https://doi.org/10.1002/jcc.21816

https://doi.org/10.26850/1678-4618.eq.v50.2025.e1600

Supplementary Information

FT-IR Analysis of the extract

FTIR spectroscopic analysis provides significant insights into the chemical composition and structural characteristics of the analyzed compounds. FT-IR (PerkinElmer Spectrum IR; Version 10.6.2) analysis of all the extracts was conducted at the Amrit Campus in Kathmandu. The spectroscopic analysis of FTIR enables the identification of functional groups found in the extracts (Grasel *et al.*, 2016). The comparative spectral peaks of extracts are presented (**Fig. 3S**). Alcohols, alkyl groups, and carbonyl groups were found most abundant in the extract fractions.

Ligand structures

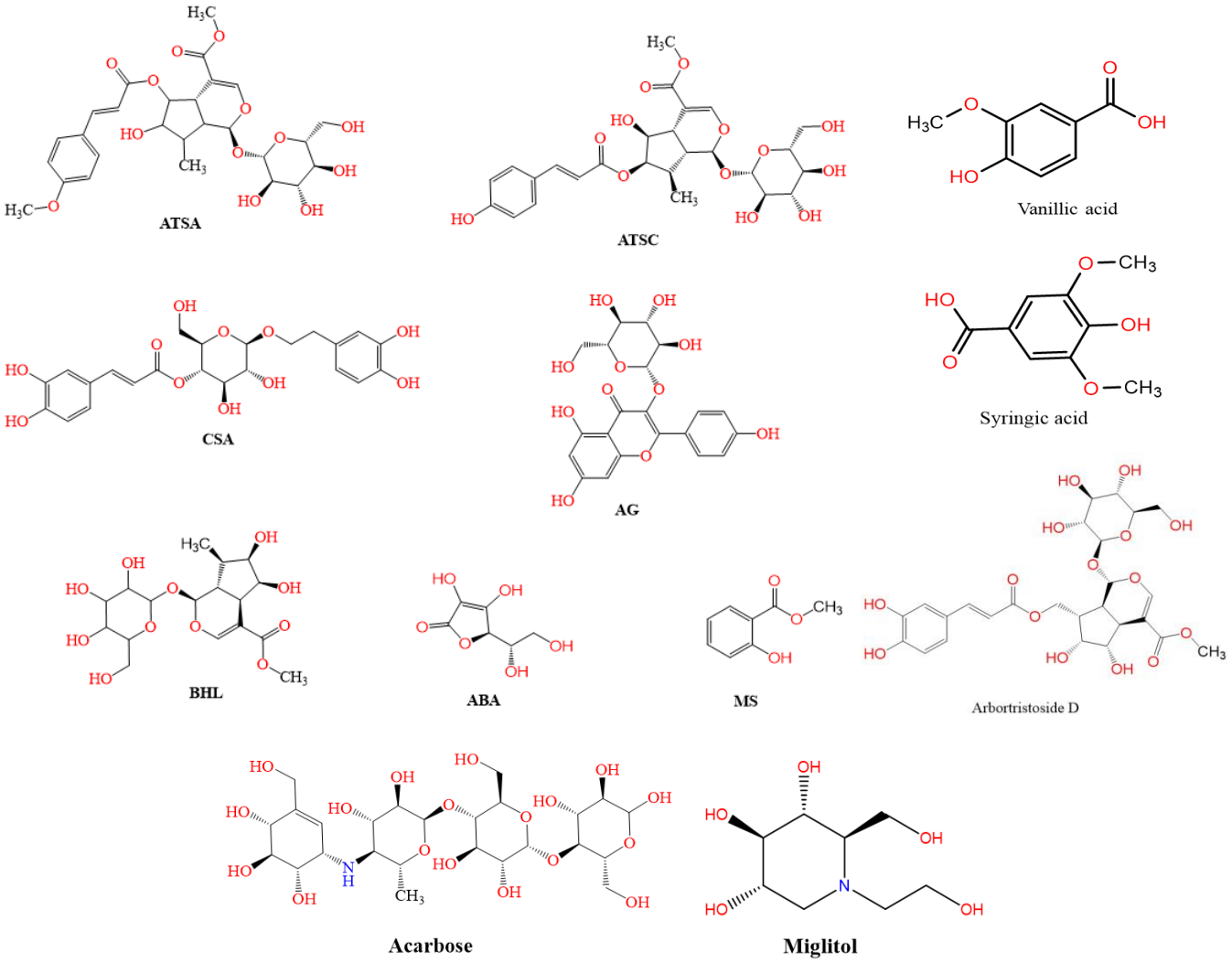

Figure 1S. Molecular structures of selected ligands for molecular docking and standard drugs (acarbose and miglitol) drawn in ChemDraw 16.
Source: Elaborated by the authors.

https://doi.org/10.26850/1678-4618.eq.v50.2025.e1600

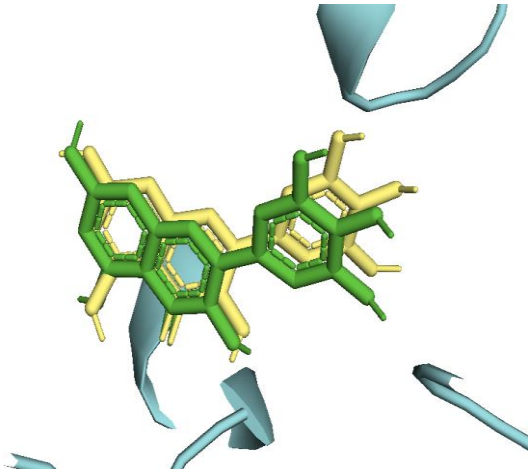

Figure 2S. (RMSD <2 Å), Superimposition of the native ligand myricetin (green) with docked ligand (yellow) myricetin, visualized in PyMOL software.
Source: Elaborated by the authors.

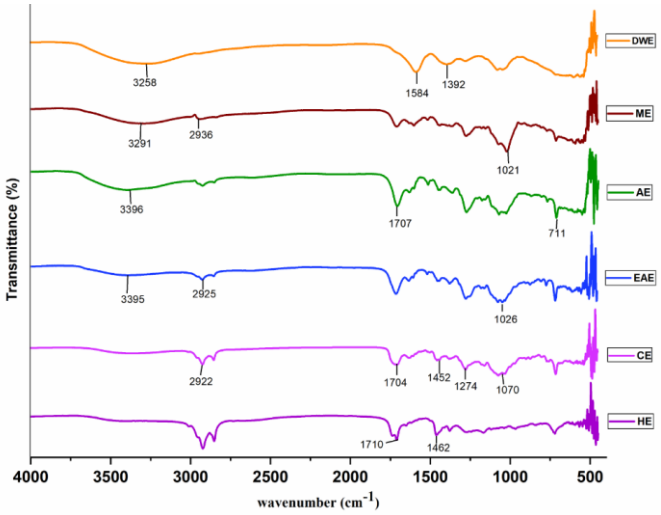

Figure 3S. FTIR analysis of extract fractions.
Source: Elaborated by the authors.

Standard calibration curves for TPC and TFC

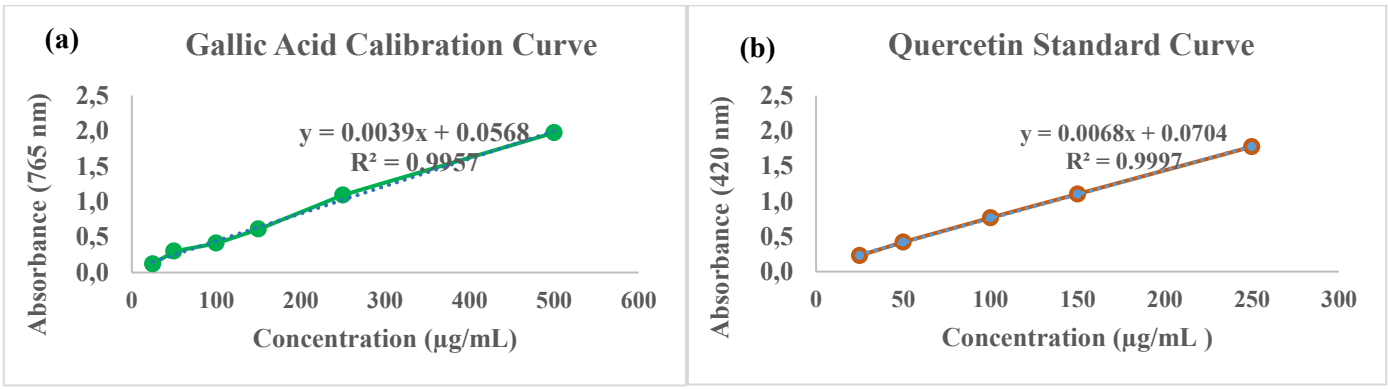

Figure 4S. Standard calibration curve of **(a)** Gallic acid and **(b)** Quercetin solution.
Source: Elaborated by the authors.

Comparative and figurative presentation of antioxidant potential of extract fractions

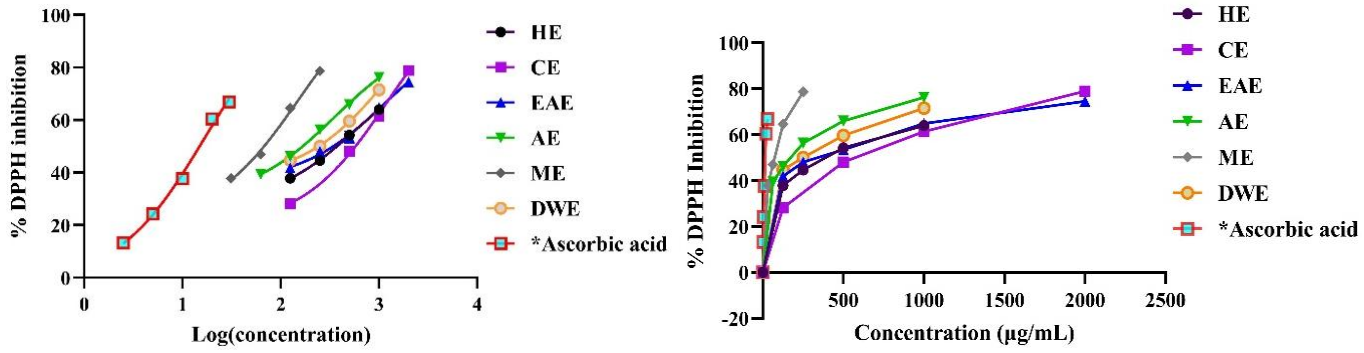

(a) (b)

Figure 5S. The comparative trending curve of DPPH assay of extracts in dose-inhibition response with **(a)** Log(concentration) vs % scavenging of DPPH and **(b)** concentration vs % scavenging with positive control ascorbic acid.
Source: Elaborated by the authors.

https://doi.org/10.26850/1678-4618.eq.v50.2025.e1600

Alpha amylase inhibition assay

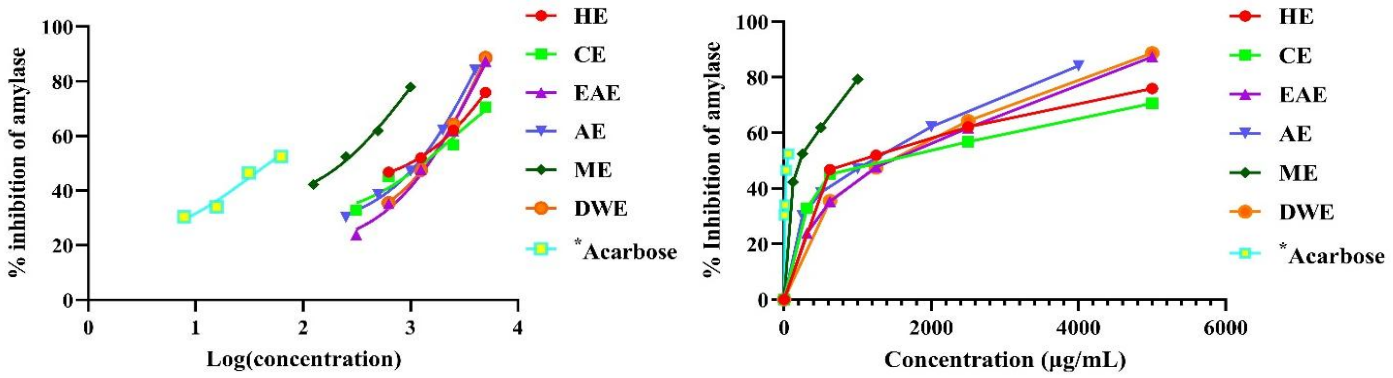

(a) (b)

Figure 6S. Nonlinear regression graphic presentation of **(a)** log(concentration) vs percentage inhibition of enzyme **(b)** Concentration vs percentage inhibition of enzyme with positive control acarbose.
Source: Elaborated by the authors.

Brine shrimp lethality assay

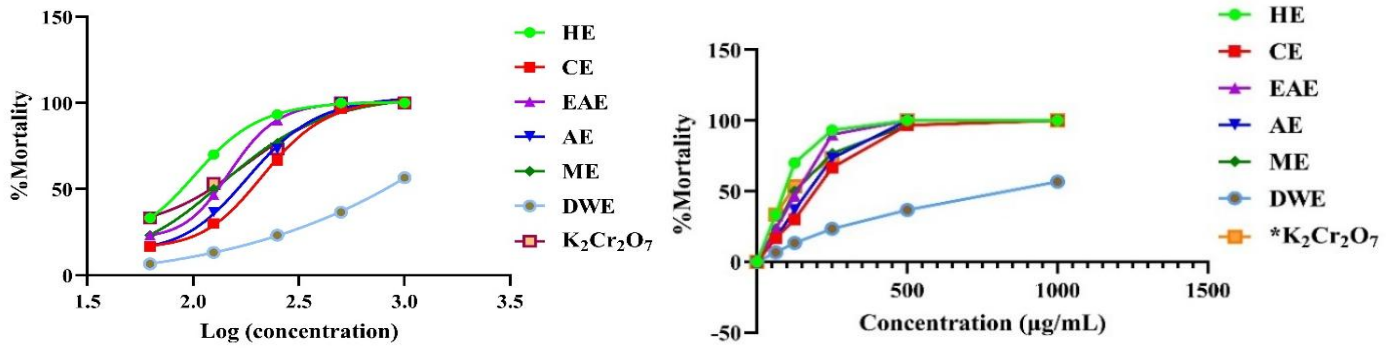

(a) (b)

Figure 7S. Nonlinear regression comparative curves of **(a)** log (concentration) vs % mortality and **(b)** concentration vs % mortality of triplicate with control, the plot is drawn from GraphPad Prism in dose-inhibition response plot.
Note: **HE** (Hexane extract); **CE** (Chloroform extract); **EAE** (Ethyl acetate extract); **AE** (Acetone extract); **ME** (Methanol extract); **DWE** (Distilled water extract).
Source: Elaborated by the authors.

Protein-ligand Interactions

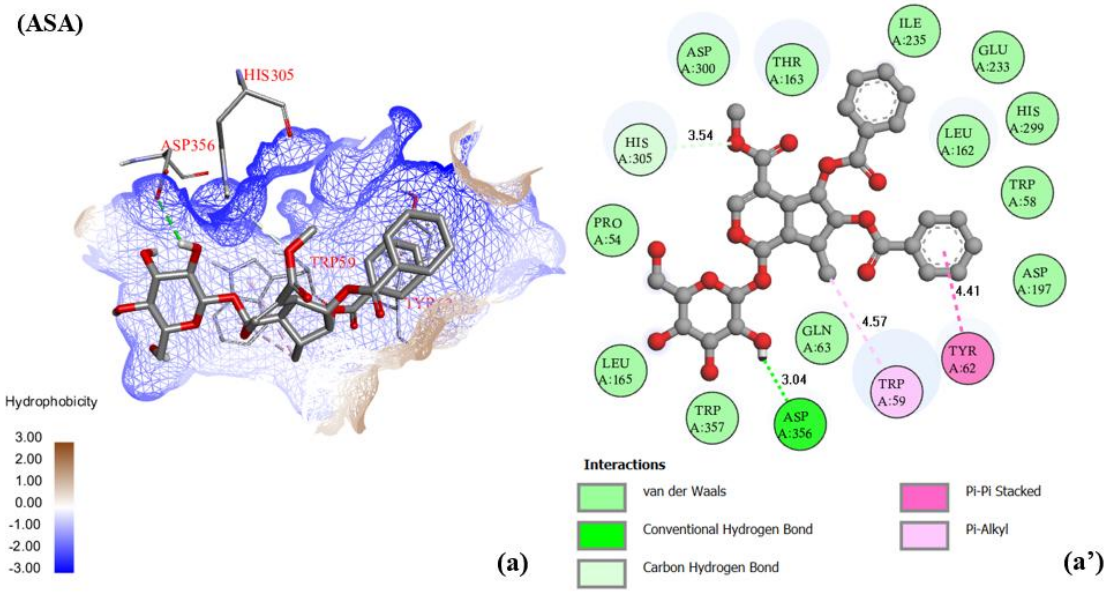

https://doi.org/10.26850/1678-4618.eq.v50.2025.e1600

(ASB)

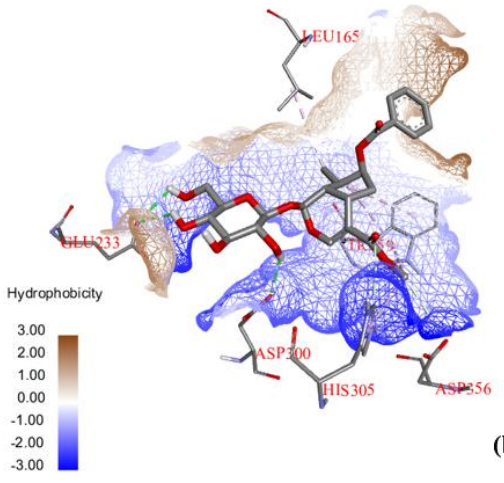

(b)

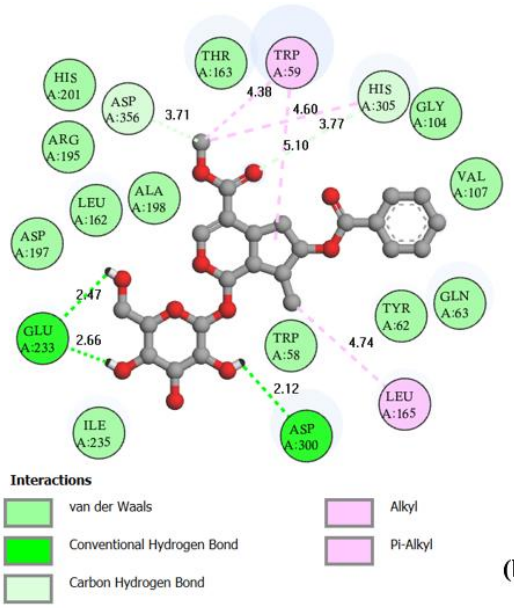

(b')

(ATSA)

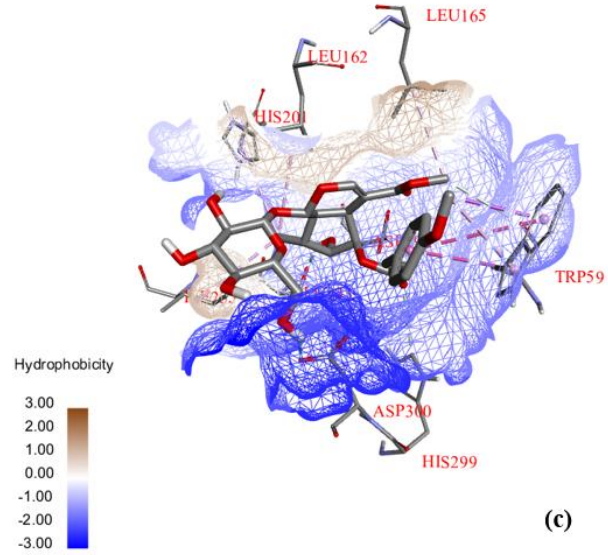

(c)

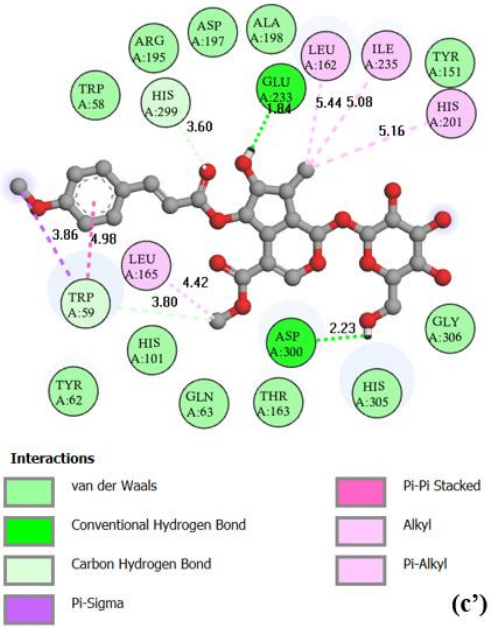

(c')

(ATSC)

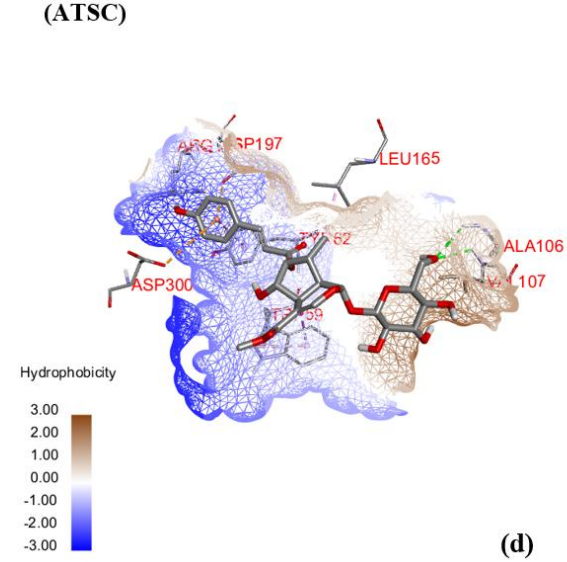

(d)

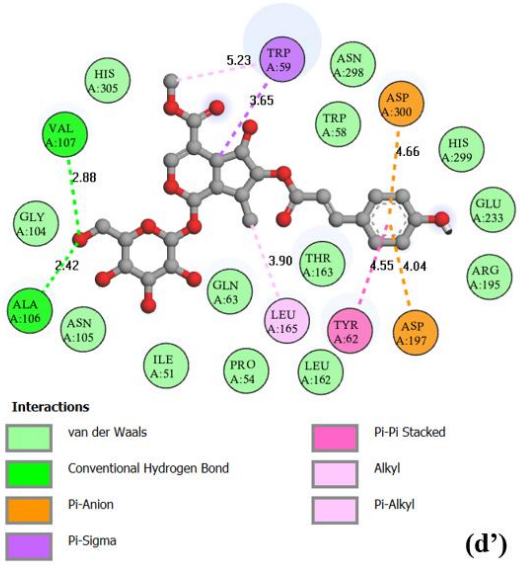

(d')

https://doi.org/10.26850/1678-4618.eq.v50.2025.e1600

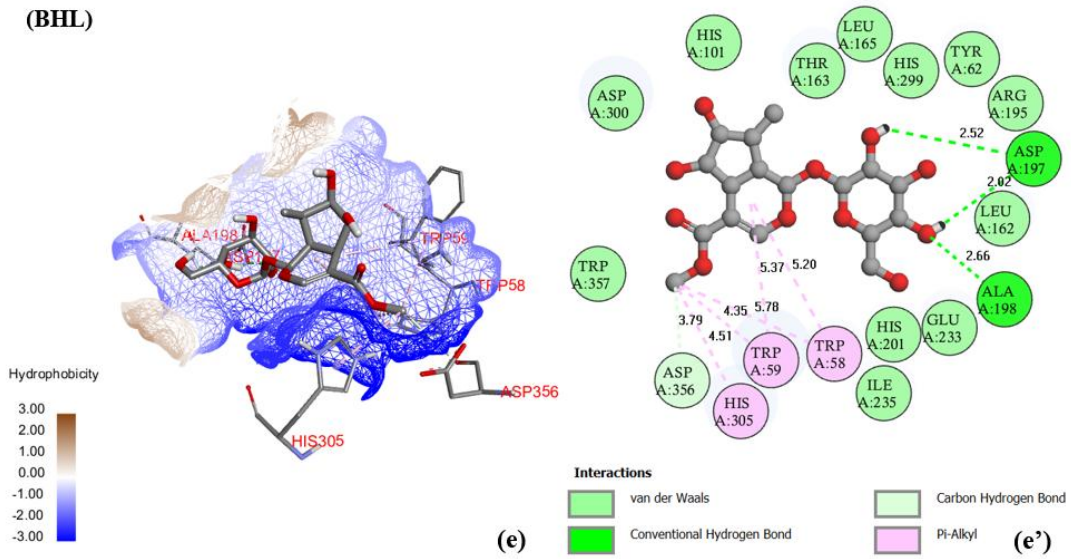

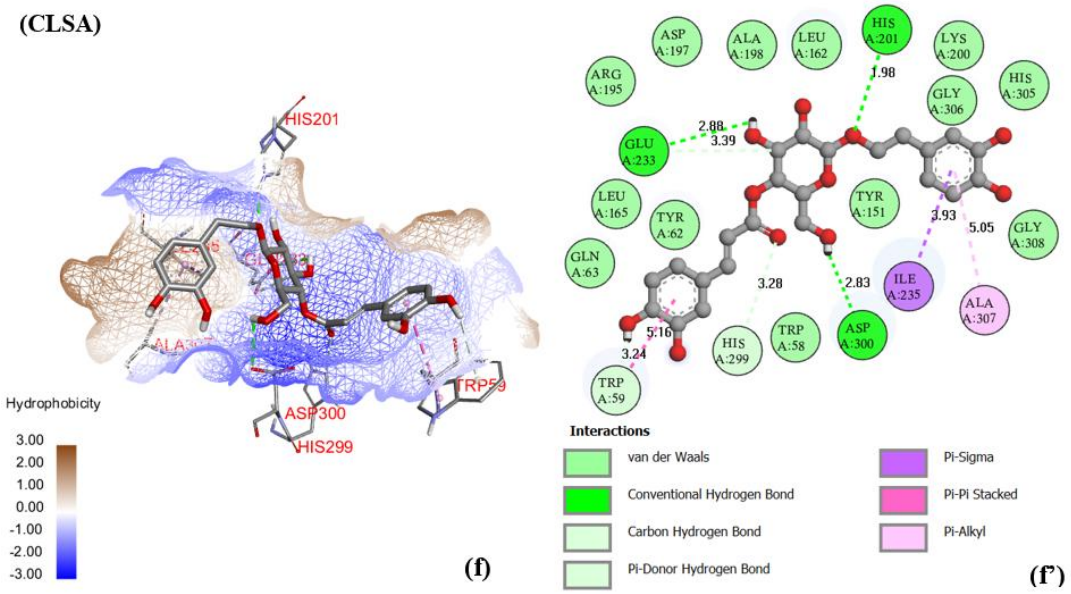

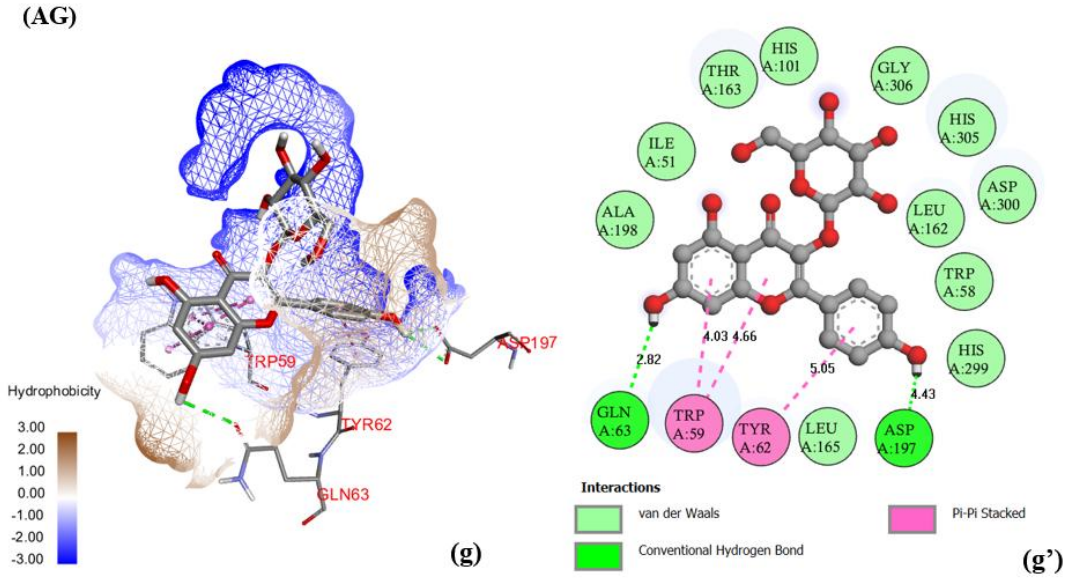

https://doi.org/10.26850/1678-4618.eq.v50.2025.e1600

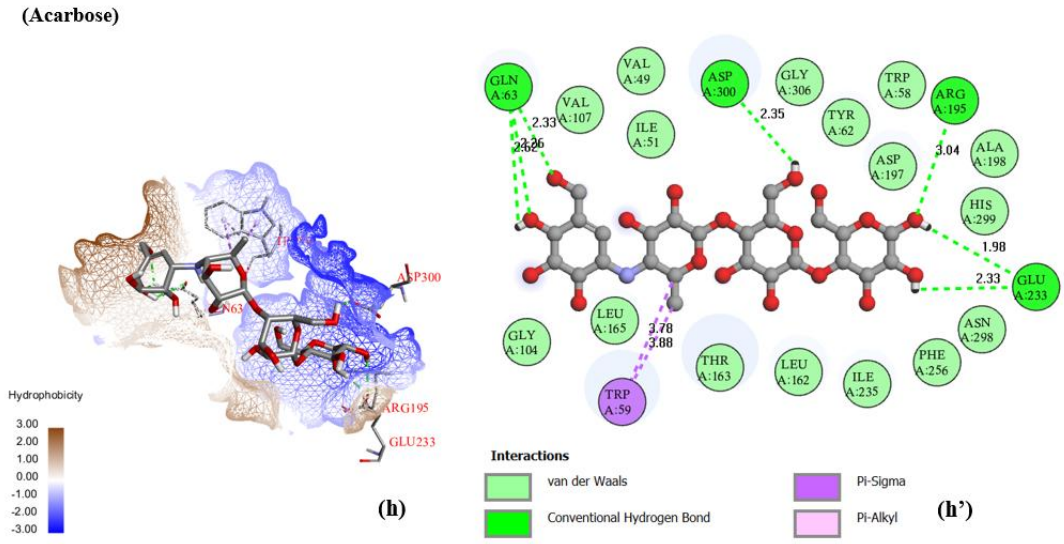

Figure 8S. 3D and 2D interactive presentations of {ASA **(a, a')**, ASB **(b, b')**, ASTA **(c, c')**, ASTC **(d, d')**, BHL **(e, e')**, CLSA **(f, f')**, AG **(g, g')**, and Acarbose **(h, h')**} with hydrophobicity in receptor protein in molecular docking.
Source: Elaborated by the authors.

Apo structure Dynamics and characterization

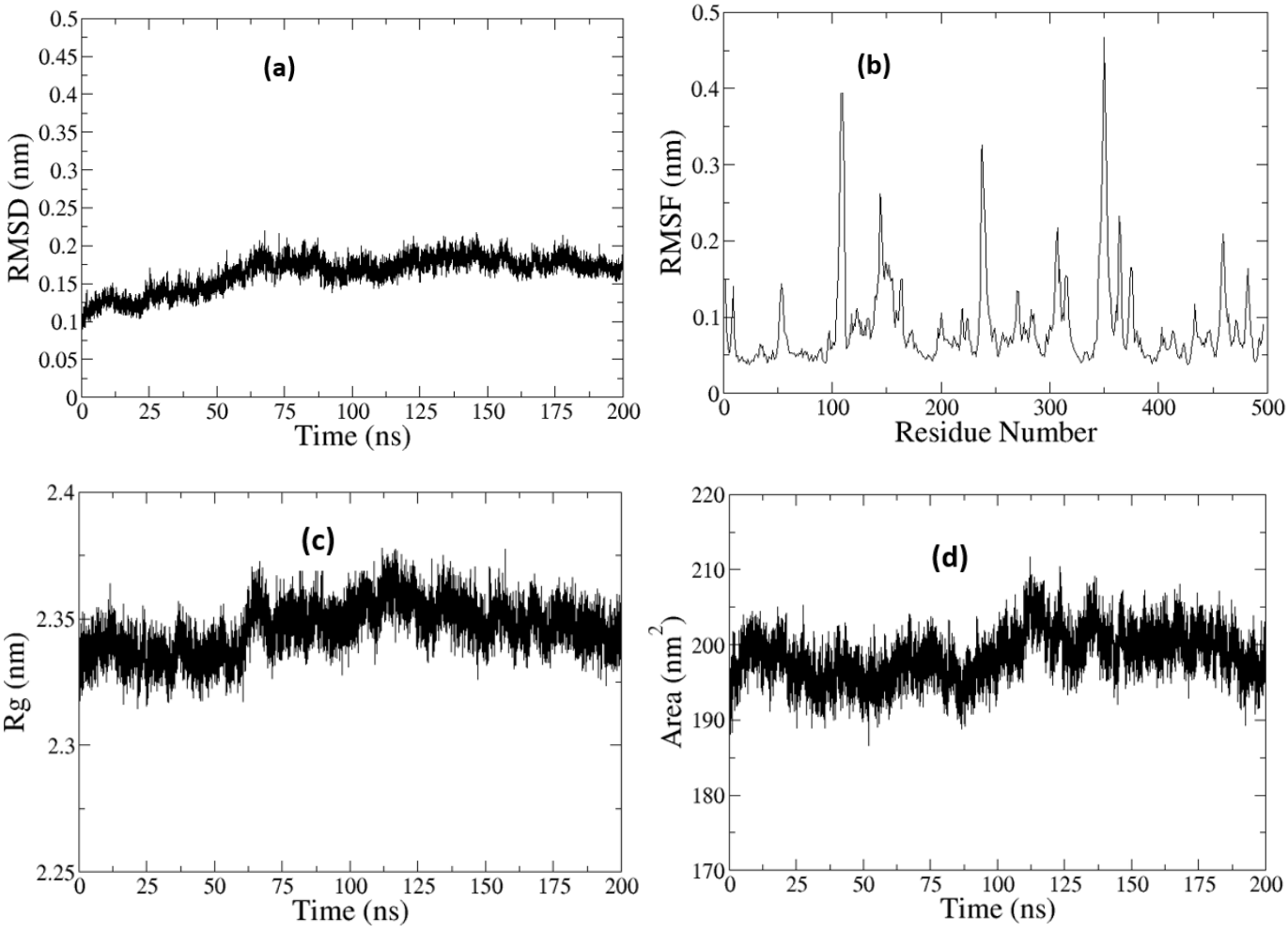

Figure 9S. Presentation of MDS of the apo structure of amylase protein (4GQR) of **(a)** RMSD **(b)** RMSF **(c)** R_g **(d)** SASA.
Source: Elaborated by the authors.

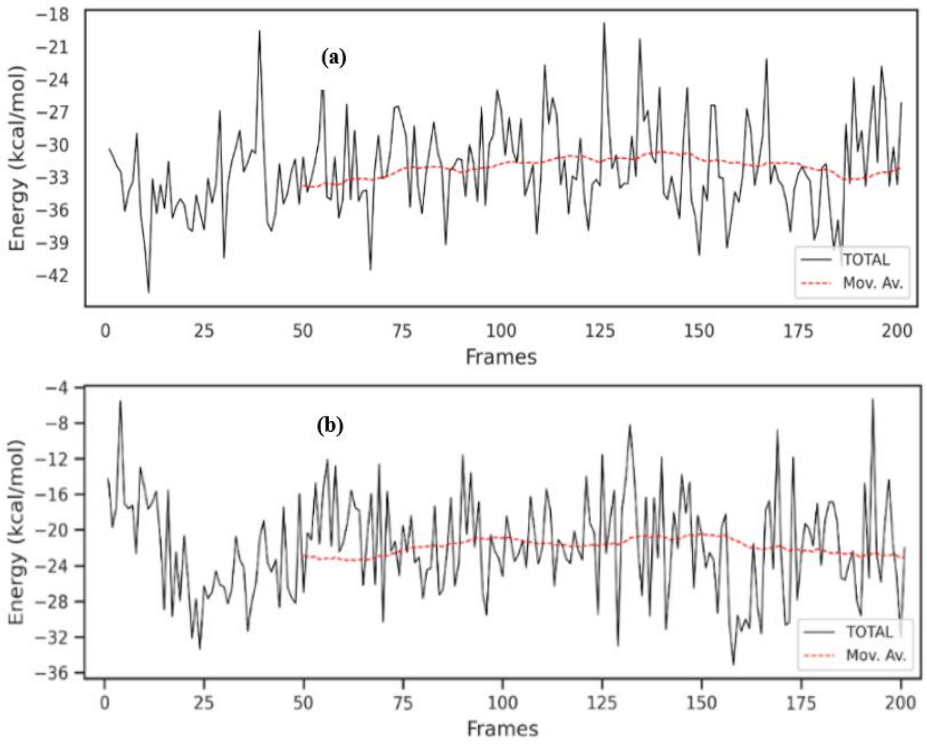

Figure 10S. Binding free energy change with respect to the time frame of the complex with ligand **(a)** ASC **(b)** ASD.
Source: Elaborated by the authors.

Table 1S. Ligands with their docking scores.

Ligands	Ligand ID	Molecular weight (g/mol)	PubChem ID	Docking score (kJ/mol)	References
6-β-Hydroxyloganin	BHL	406.4	341846	−29.7	Rathore *et al.*, (1989)
Calceolarioside-A	CLSA	478.4	5273566	−32.6	Agrawal and Pal (2013); Dewi *et al.* (2022)
Ascorbic acid	ABA	176.12	54670067	−22.6	Agrawal and Pal (2013); Sah and Verma (2012)
Methyl salicylate	MSC	152.15	4133	−23.0	
Arbortristoside D	ATSD	584.5	14632886	−32.6	Agrawal and Pal (2013)
Vanillic acid	VA	168.15	8468	−33.0	Agrawal and Pal (2013); Sah and Verma (2012)
Syringic acid	SA	198.17	10742	−24.3	

Source: Elaborated by the authors.

Table 2S. Detailed information about some ligands containing docking scores, type of interactions and active site residues involved.

Candidates	Docking score (kJ/mol)	Interactions	Active site residues (Distance Å)
ASA	−32.6	Conventional H-bond	ASP356 (3.04)
		Pi-Pi Stacked	TYR62 (4.41)
		Pi-Alkyl	TRP59 (4.57)
		Carbon-Hydrogen Bond	HIS305 (3.54)
		van der Waals	PRO54, TRP58, GLN63, LEU162, THR163, LEU165, ASP197, GLU233, ILE235, HIS299
CLSA	−32.6	Conventional Hydrogen Bond	HIS201 (1.98), GLU233 (2.88), ASP300 (2.83)
		Pi-Alkyl	ALA307 (5.05)
		Carbon Hydrogen bond	TRP59 (3.24)
		Pi-Pi Stacked	TRP59 (5.16)
		Pi-sigma	ILE235 (3.93)
		Pi-Donor Hydrogen bond	HIS299 (3.28)
		van der Waals	TRP58, TYR62, GLN63, TYR151, LEU162, ARG195, ASP197, ALA198, LYS200, HIS305, GLY306, GLY308
ATSC	−31.4	Conventional Hydrogen Bond	ALA106 (2.42), VAL107 (2.88)
		Pi-Alkyl	TRP59 (5.23)
		Pi-Anion	ASP197 (4.04), ASP300 (4.66)
		Pi-Pi Stacked	TYR62 (4.55)
		Pi-sigma	TRP59 (3.65)
		Alkyl	LEU165 (3.90)
		van der Waals	ILE51, PRO54, TRP58, GLN63, LEU162, THR163, LEU165, ARG195, GLU233, HIS299, ASN298, HIS305

Continue...

BHL	−29.7	Conventional H-bond	ASP197 (2.02, 2.52), ALA198 (2.66)
		Pi-Alkyl	TRP58 (5.20, 5.78), TRP59 (4.35, 5.37), HIS305 (4.51)
		Carbon-Hydrogen Bond	ASP300 (3.79)
		van der Waals	TYR62, HIS101, LEU162, THR163, LEU165, ARG195, HIS201, GLU233 ILE235, ASP300, TRP356, TRP357

Note: **ASA** (arborside-A); **CLSA** (Calceolarioside-A); **ATSC** (arbortristoside-C); **BHL** (6-β-Hydroxyloganin).
Source: Elaborated by the authors.

References

Agrawal, J.; Pal, A. *Nyctanthes arbor-tristis* Linn - A Critical Ethnopharmacological Review. *J. Ethnopharmacol.* **2013**, *19*, 645–658. https://doi.org/10.1016/j.jep.2013.01.024

Dewi, N. K. S. M.; Fakhrudin, N.; Wahyuono, S. A Comprehensive Review on the Phytoconstituents and Biological Activities of Nyctanthes Arbor Tristis L. *J. Appl. Pharm. Sci.* **2022**, *12* (8), 9–17. https://doi.org/10.7324/JAPS.2022.120802

Grasel, F. D. S.; Ferrão, M. F.; Wolf, C. R. Development of Methodology for Identification the Nature of the Polyphenolic Extracts by FTIR Associated with Multivariate Analysis. *Spectrochim. Acta A Mol. Biomol. Spectrosc.* **2016**, *153* (2016), 94–101. https://doi.org/10.1016/j.saa.2015.08.020

Rathore, A.; Juneja, R. K.; Tandon, J. S. An Iridoid Glucoside Form *Nyctanthes arbor-tristis*. *Phytochemistry*. **1989**, *28* (7), 1913–1917. https://doi.org/10.1016/S0031-9422(00)97886-5

Sah, A. K.; Verma, V. K. Review Paper Phytochemicals and Pharmacological Potential of *Nyctanthes arbor-tristis*: A Comprehensive Review. *Int. J. Res. Pharm. Biomed. Sci.* **2012**, *3* (1), 420–427.